Variation of the hydroxyl near infrared airglow at Rothera, Antarctica (68 °S, 68 °W)

Harald Lund

June 14, 2010

Acknowledgements

This report is the product of FY3900, Master thesis in Physics, as a partial fulfillment of the requirements to achieve a Masters degree at the Institute of Physics, NTNU. I would like to thank Prof. Patrick J. Espy for his help and guidance during this work. I woould also like to thank the British Antarctic Survey for providing the data used. Finally I would like to thank the guys at my study-room who always seemed to have done, and found the solutions to, the very same LaTeX errors as I did.

Abstract

The strongest background for astronomical observations in the infrared spectrum is hydroxyl airglow orginating from rotation-vibration transissions in the excited hydroxyl molecule. Ground based measurements of the brightness of the OH Meinel (4,2) and (3,1) band have been carried out at Rothera (68 °S, 68 °W) from 2002 to 2009. From these measurements, the temperature at the emitting heights has also been derived. This thesis explores the variations of the radiance and temperature on diurnal, seasonal and solar cycle time scales. The data displayed unevenly spaced gaps due to natural conditions like cloudy weather and the sunlight Antarctic summer.

In order to determine the trends, super-posed epoch analysis and the Lomb-Scargle periodogram were used. Both the radiance and temperature displayed decreasing values with decreasing solar activity. The seasonal behaviour of the radiance and temperature was characterized by strong summer minima and two peaks at the equinoxes, with the fall peak as the largest. On a nightly basis, the highest values were found approximately during the first five hours after sunset for the radiance. Astronomical observations in the infrared region should be carried out when the hydroxyl radiance has the lowest values. Thus such observations at the South Pole should be done in the winter time between the two equinox peaks in the radiance and more than five hours after sunset. In addition, observations done in solar cycle minima will have smaller background radiance.

Contents

1 Introduction

At night the hydroxyl radical (OH) is produced natrually in the atmosphere. The main reaction responsible for the production of excited hydroxyl is:

$$H + O_3 \rightarrow OH^* + O_2 \tag{1.1}$$

Only the highest vibrational levels of OH* are produced by this reaction. Collisional quenching or cascading produces the hydroxyl in lower vibrational levels. When the molecule cascades to lower vibrational levels, light in the infrared and near-infrared region is produced. This light is the strongest source of light in the night sky. A summary of 55 vertical profiles, obtained by 34 rocket flights, of the emission rate of the OH infrared airglow has been done by [Baker and Stair 1988]. The result of this summary is that the hydroxyl radical is found in a relatively thin layer, about 8 kilometers thick, situated at a nearly constant altitude of 87 kilometers. The infrared radiation produced in this layer can be observed from the ground. Given its brightness and thermal equilibrium with the surrounding atmosphere, ground-based spectroscopic studies of the hydroxyl nightglow have been used extensively to infer the atmospheric temperature near 87 km as well as the temperature perturbations produced by large- and small-scale dynamic processes occurring there.

1.1 Astronomical observations in the infrared

While this makes hydroxyl ideal for remote sensing of the temperature and dynamics of this atmospheric region, it also represents the strongest background through which astronomers must try to observe faint infrared sources [Iwamuro et al. 1994], [Maihara et al. 1993]. In the 1-2.2 μm range, the space infrared sky is a thousand times fainter than the OH airglow [Wright 2005]. Beyond 2.4 μm, thermal emission is the dominant background for astronomical observations [Content 2005]. The infrared region of the spectrum, with its ability to sense cool objects and to see through interstellar dust, is particularly well suited to planetary detection and galactic astronomy. The cold, dry and stable conditions of Antarctica makes it well suited for such observations. Therefore there are new international efforts to construct observatories there. However the variability of the main backround to any astronomical observations in the infrared, the hydroxyl emission, is not well characterized there.

Different methods can be used to remove the background caused by hydroxyl radiation. With high spectral resolution, the OH spectra is composed of numereous narrow lines, often with gaps considerably larger than

the line width. Therefore it is possible to remove the hydroxyl emissions from measurements in the infrared. Different methods to achieve this have been proposed by [Iwamuro et al. 1994], [Content 2005], [Corbett et al. 2007] and [Davies 2006]. None of these methods are perfect. Removal of the OH lines will typically decrease the signal to noise ratio. Further some of the methods are not able to remove all OH lines. Therefore it is still of importance to make measurements when the hydroxyl display the smallest values. To find the periods with lowest hydroxyl airglow, this thesis will explore the variation in the hydroxyl airglow within the H-band atmospheric window (1475-1825nm) at wavelengths 1582 and 1505 nm respectively, at Rothera, Antarctica (68 °S, 68 °W).

1.2 Hydroxyl airglow variation

Measurements of the OH Meinel (4,2) and (3,1) bands have been made in the time period from 2002 to 2009. These bands and their lines represents the frequencies produced by rotational-vibrational transitions from vibrational level $v = 4$ to $v = 2$ and $v = 3$ to $v = 1$. All vibrational levels of excited hydroxyl and in turn their radiation are proportional to the concentration of atomic oxygen. Thus the radiation from the two bands investigated will be representative of the total radiative emission of excited hydroxyl. Emissions from hydroxyl are found to vary on diurnal, [Mulligan et al. 1994, Marsh et al. 2006], on seasonal, [Le Texier et al. 1987] and on solar cycle, [Espy and Stegman 2002] time scales. In this thesis super-posed epoch analysis will be used to construct the nightly variation as a function of season. Furthermore the seasonal and solar cycle variation will be investigated. Thus astronomical observations can be made when the hydroxyl airglow displays its lowest values.

Along with the measurements of the radiation of the two OH bands, measurements of the temperature have been made. The processes leading to changes in the radiation also influence the temperature at the hight of the hydroxyl layer. Thus similar variations is found in the temperature as in the radiance [Azeem et al. 2007, Espy and Stegman 2002, Pan and Gardner 2003]. In addition to this, the techniques used to determine the variation in the radiation can be used to determine the variation in the temperature. Therefore the variation on a nightly, seasonal and solar cycle timescale is examined. Finally the connection between temperature and radiance for the two bands is investigated.

1.3 Progress of this text

The thesis is buildt up in the following way. First the quantum mechanical srtucture of the OH molecule is presented. Next the atmospheric structure and the processes causing the formation and destruction of hydroxyl in the different vibrational levels is shown. Finally the methods used to obtain the raw data is explained. These methodes and processes are presented in chapter 2. In chapter 3 the techniques used to determine the long term variation in the temperature and radiance, both on seasonal and solar cycle time scales, are described along with the results obtained using them. Further the diurnal variations in the radiation and temperature are presented. Finally the connection between temperature and radiance is investigated. In chapter 4 the underlying processes for the trends in the variation are examined. Finally the optimal observation periods for astronomical observations in the near-infrared and infrared region with regard to the OH-airglow background are presented.

2 Theory

In order to understand the origin of the hydroxyl airglow in the night sky, a basic understanding of the quantum mechanical structure of the OH molecule and the quantum mechanical transitions taking place in the molecule is needed. To give the reader such an understanding, the basic structure of the OH molecule is presented in this chapter. In addition, the chemistry responsible for the production and destruction of excited hydroxyl is outlined along with the atmospheric structure. Finally a brief overwiev of the instrumentation is given.

2.1 The OH-layer

The Earth's atmosphere is divided into separate vertical layers classified by the temperature gradient. [Andrews 2000] gives the following structure of the Atmosphere. The layer from the ground to about 15 km alltitude is called the troposphere and is bounded above by the tropospause. Here the temperature gradient is negative, i.e. the temperature decreases with increasing altitude. The decrease is due to solar heating of the ground which will cause highest values near the ground. Above the troposphere, from about 20 km alltitude to 50 km alltitude, lies the stratosphere. In this region of the atmosphere the temperature gradient is positive, which is caused by direct heating of the ozone. In the same way as the troposphere is bounded by the tropospause, the stratosphere is bounded by the stratospause. Following the stratosphere comes the mesosphere, bounded above by the mesopause covering the altitude from 50 km to about 90 km. Here the temperature gradient is again negative. The negative gradient is caused by decreased solar heating and increased radiative cooling to space. Finally comes the thermosphere, in which the temperature gradient changes one more time from negative to positive. This is because high energetic solar radiation is absorbed by the small amount of molecular oxygen still present. This structure is shown in figure 2.1. Centered around 87 km in a relatively thin emitting layer of 6-8 km exited hydroxyl (OH*) is produced naturally, mainly by the reaction. [Baker and Stair 1988, Marsh et al. 2006, Lowe et al. 1996]:

$$H + O_3 \rightarrow OH^* + O_2 \tag{2.1}$$

Thus the production rate of OH* is:

$$P(OH^*) = k_{H+O_3}[H][O_3] \tag{2.2}$$

At night, this reaction constitutes the major loss of ozone, and in steady state may be equated to the production rate of ozone. The production of

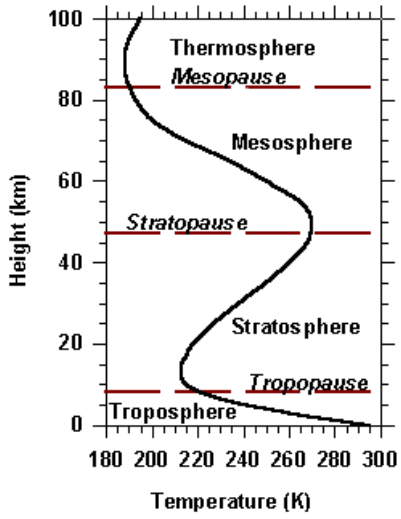

Figure 2.1: Vertical structure of the atmospheric temperature. The figure is from [CRISP].

ozone is a result of recombination with atomic oxygen through the reaction:

$$M + O + O_2 \rightarrow O_3 + M \tag{2.3}$$

At night this reaction represents the major production of ozone. The O_3 concentration at night is determined by setting the production due to recombination of atomic oxygen equal to losses by reactions with atomic hydrogen [Marsh et al. 2006] such that:

$$[O_3] = \frac{k_{O+O_2+M}[O][O_2][M]}{k_{H+O_3}[H]} \tag{2.4}$$

By substituting equation (2.4) into equation (2.2), one obtains for the production of exited hydroxyl:

$$P(OH^*) = k_{O+O_2+M}[O][O_2][M] \tag{2.5}$$

Thus it is clear that the concentration of exited hydroxyl is ultimately proportional to the atomic oxygen concentration. It is also evident that both the ozone concentration and the concentration of exited hydroxyl are proportional to the atomic oxygen concentration. Atomic oxygen in the mesosphere is created by photolysis of ozone through the reaction [Ditky et al. 2010].

$$O_3 + light \rightarrow O_2 + O \tag{2.6}$$

As sunlight needs to be present to produce atomic oxygen, no such production occurs during the night. Then process (2.6) in sunlit regions, followed by horizontal and vertical transport, are the mechanisms able to change the concentration of atomic oxygen at night.

2.2 The OH-molecule

In the following chapter the origin for the OH Meinel bands will be explained. The material regarding the quantum states of diatomic molecules is covered in [Herzberg 1971] and [Herzberg 1950]. This chapter is intended to give the reader an idea of which quantum mechanical transitions that give rise to the OH Meinel (3,1) and (4,2) band. These are the two bands discussed in this thesis. An atom or a molecule cannot exist in states with arbitrary energy. The energy states can only take certain discrete values. These possible energystates are determined by the quantum conditions of the atom. As an example one can look at the hydrogen atom. A hydrogen atom is a single electron bound to a single proton by the Coloumb field. Classically the electron can move in eliptical orbits around the proton. Depending on how strongly the electron is bound to the proton, the orbits can have any axes and give a continious energy-spectrum. This is shown not to be the case. As mentioned, the energy levels are discrete. This can only be explained by quantum mechanics, which give the following values [Hemmer 2005] for the energy levels of the hydrogen atom:

$$E_n = -\frac{m}{2\hbar^2}\left(\frac{Ze^2}{4\pi\epsilon_0}\right)\frac{1}{n^2}, n = 1, 2, ... \tag{2.7}$$

Where $m = m_1 m_2/(m_1 + m_2)$ is the reduced mass of the system, and n is the quantum number characterizing the electronic energy. The zero level energy is set to be when the electron is completely separated from the proton and has zero kinetic energy. When the the atom makes a jump from one discrete energy value to another, the energy-difference can be carried away by an emitted photon if the atom jumps to a lower level. If the atom jumps to a higher level, the energy can come from an absorbed photon. The photons energy and frequency will be decided by the energy difference between the subsequent levels. Thus the photon will have the energy:

$$h\nu = E_n - E_k = \left(\frac{e^2}{4\pi\epsilon_0}\right)\frac{m}{2\hbar^2}\left(\frac{1}{k^2} - \frac{1}{n^2}\right) \tag{2.8}$$

Since the electrons angular momentum is also quantized in units of $\sqrt{l(l+1)}\hbar$, l can take the discrete values $0, 1, 2, ..., n-1$ with n being the main quan-

tum number. Relatvistic corrections give a splitting in the energy levels that results in a splitting in the allowed photon energy.

For diatomic molecules the situation is more complex. In addition to the electronic energy, both the rotational and the vibrational energy of the molecule will be quantized. Then the energy of the molecule can be represented by the sum of the three parts:

$$E = E_e + E_v + E_r \tag{2.9}$$

As a simple model of the rotation of the molecule, the dumbbell model can be used. In this model the molecule consists of two mass points with masses m_1 and m_2 connected by a massless rod with length r. Classically the rotational energy of this kind of model is given by:

$$E_r = \frac{1}{2} I \omega^2 \tag{2.10}$$

As with the electronic states of the hydrogen, quantum mechanics only allow certain discrete values of the rotational energy. With the dumbbell model these are given by:

$$E_r = \frac{h^2}{8\pi^2 \mu r^2} J(J+1) \tag{2.11}$$

J is the rotational quantum number and can take the values $0, 1, 2, ...$ The reduced mass of the system is given by μ. As for the electronic spectra of the hydrogen atom, the molecule can go from one rotational state to another by emitting or absorbing a photon. A photons energy is given by:

$$E_n - E_k = \Delta E = h\nu = \frac{hc}{\lambda} \Rightarrow \frac{1}{\lambda} = \frac{\Delta E}{hc} \tag{2.12}$$

With λ beeing the photons wavelength. To get the inverse wavelength of the emitted/absorbed photon, the rotational energy is given by the so called term values determined by:

$$F(J) = \frac{E_r}{hc} = BJ(J+1), B = \frac{h}{8\pi^2 c \mu r^2} \tag{2.13}$$

B is called the rotational constant. If the molecule is not completely rigid, the centrifugal force will give rise to a small correction term, but this term is always much smaller than the rotational constant. The rotational constant of OH is greater than for example NO_2 and N_2, but still a factor of 10^4 smaller than B.

As mentioned above, the molecule will also have vibrational energy. In a first approximation, the vibrations of the molecule can be represented by a

harmonic oscillator. A harmonic oscillator is a system consisting of a mass point under the action of a restoring force proportional to the displacment from an equlibrium point. With μ as the reduced mass, the motion of the two nuclei can be represented by the motion of a single particle. The displacement is given by $r - r_e$ where r is the distance between the nuclei and r_e is the equlibrium distance. For a harmonic oscillator the quantum mechanical energy is given by:

$$E_\nu = \nu_{osc}(v + 1/2), v = 0, 1, 2, ... \tag{2.14}$$

where v is the vibrational quantum number. The energy are given by the term values:

$$G(v) = \frac{E_v}{hc} = \omega(v + 1/2) \tag{2.15}$$

The molecule is, in fact, not a strictly harmonic oscillator, but an anharmonic oscillator. Taking this into consideration the term values of the vibrational levels ($v = 0, 1, \cdots$) are given by:

$$G_0(v) = \omega_0 v - \omega_0 x_0 v^2 + \omega_0 y_0 v^3 + ... \tag{2.16}$$

where $\omega_0 x_0, \omega_0 y_0, ...$ are in general smal compared to ω_0. Thus the displacement between the energy levels decreases with increasing v. In contrast the displacement berween the energy levels of a strictly harmonic oscillator are constant. Since the rotational constant from equation (2.13) depends on the distance r between the nuclei, it is not strictly a constant. Different vibration levels will have different r-values. Therefore B must be replaced by B_v with v refering to the different vibrational levels of the molecule.

A pure vibration spectrum is where the molecule makes a transition from one vibration level to another. If one also takes into consideration the fact that the molecule can change its rotational level at the same time, one obtains the rotation-vibration spectrum. The various rotational transitions that can take place in a given vibrational transition give rise to so called rotation-vibration bands. The OH Meinel (4,2) and (3,1) bands are examples of such bands. To get the inverse wavelength of these kind of bands, the term values from both the rotational and the vibrational part have to be added. The vibrational part is given by equation (2.16):

$$v_v = G(v') - G(v'') \tag{2.17}$$

The rotational part is given by:

$$v_r = F_{v'}(J') - F_{v''}(J'') \tag{2.18}$$

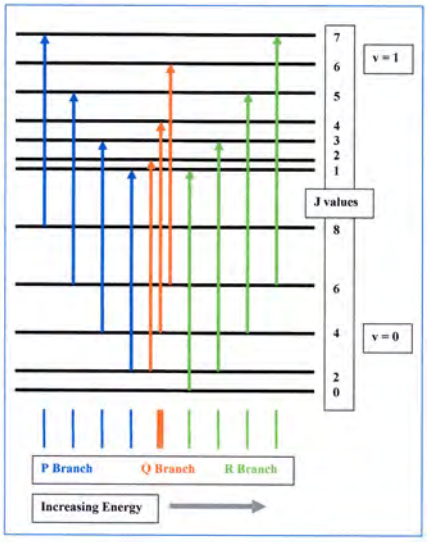

Figure 2.2: Possible rotational transitions for a $v = 0$ to $v = 1$ vibrational transition, the figure is from [Barrett 2010]. for clarity only even levels are shown for for the lower state.

Substituting into equation (2.13) and combining the rotational and vibrational part one obtains.

$$v = v_v + B'J'(J'+1) - B''J''(J''+1) \tag{2.19}$$

Where the subscript v has been omitted from B' and B''. Quantum mechanical selection rules puts certain constraints on $\Delta J = J' - J''$, namely that.

$$\Delta J = 0, \Delta J = \pm 1 \tag{2.20}$$

Substituting this into (2.19), writing J instead of J'' and $\Delta J = 0$, one obtains an inverse wavelength given by.

$$v_Q = v_v + (B' - B'')J + (B' - B'')J^2 \tag{2.21}$$

The branch of lines with $\Delta J = 0$ are refered to as the Q-branch. The branch with $\Delta J = 1$ and $J' = J + 1$ is called the R branch while the branch with $\Delta J = -1$ and $J' = J - 1$ is called the P-branch. Again substituting into equation (2.19), v for these two branches is given by.

$$v_R = v_v + 2B' + (3B' - B'')J + (B' - B'')J^2 \tag{2.22}$$

$$v_P = v_v - (B' + B'')J + (B' - B'')J^2 \tag{2.23}$$

A schematic picture of the the allowed rotational transitions for the vibrational transition $v = 0$ to $v = 4$ is given in figure 2.2. When one also takes into account the motion of the electrons of the molecule, corrections to the simple dumbbell model arise. These corrections give rise to a splitting in the rotational levels. This splitting is determined by which electronic state the molecule is in. The molecule can have angular momentum $\Lambda = 1/2$ or $\Lambda = 3/2$. Transitions between the the two states with different Λ give rise to a splitting of the bands. Photons created by a transition with the same ΔJ can have different frequency due to the difference in Λ. This is the origin of the different lines in a given band. In 1950 [Meinel 1950] observed the rotation-vibration spectrum from OH in the night sky. Although he first believed this was a representation of a new electronic band system, it soon became clear that the bands were in fact rotation-vibration bands, with the P, Q and R branches being observed.

2.3 Concentration of the different vibrational levels

Reaction (2.1) can produce OH* with v as high as 9 [Sivjee 1991]. Further, only levels $v = 6$ to $v = 9$ are produced with the levels 8 and 9 as the most probable. [Sivjee 1991, Le Texier et al. 1987]. Lower vibrational levels are produced when the exited molecule cascades down by radiating to lower vibrational states by vibrational and rotational transitions. If the excited hydroxyl molecule collides with another atom or molecule, it may transfer some or all of its vibrational energy to kinetic energy in this atom or molecule. This process will also lower the vibratioal level and contribute to the production of hydroxyl in the lower vibrational levels. Such a process is called collisional quenching. In this way hydroxyl in the vibrational levels 4 and 3 are produced. These levels can radiate further down with $\Delta v = 2$ to the vibrational levels 2 and 1. This is the orgin of the OH Meinel (3,1) and (4,2) bands.

Collisional quenching and transitions will contribute to the concentration of excited hydroxyl with vibrational level smaller than 8. Inserting equation (2.4) for the concentration of ozone into equation (2.2) gives the following expression for the production rate of vibrational level 8 and 9 of OH*:

$$P(OH^*)_v = k_{O+O_2+M}[O][O_2][M] \tag{2.24}$$

The lower levels will be produced by cascade through collisional quenching and direct radiation from the levels produced by (2.24) Since the highest levels are proportional to the atomic oxygen concentration the concentration of all the levels of OH* will be proportional to the concentration of atomic

oxygen. At nighttime when there is no dissociation of ozone by light, losses of a given vibrational level of excited hydroxyl are the sum of cascade terms and direct losses through the reactions:

$$OH_v^* + O \rightarrow H + O_2 \tag{2.25}$$

$$OH_v^* + O_2 \rightarrow OH_{v-1}^* + O_2 \tag{2.26}$$

$$OH_v^* + CO_2 \rightarrow OH_{v-1}^* + CO_2 \tag{2.27}$$

(2.25) represents the direct loss while (2.26) an (2.27) represent losses through cascade. When direct radiation is included, the total loss of a given vibrational level, v, is given by:

$$L(OH_v^*) = \left(\sum_{v'<v} A_{vv'} + k_v^1[O] + k_v^2[O_2] + k_v^3[CO_2] \right) [OH_v^*] \tag{2.28}$$

The term $\sum_{v'<v} A_{vv'}$ represents transitions from vibrational level v to a lower vibrational level v'. $A_{vv'}$ are the Einstein coefficients describing the probability for a given transition to occur through dipole radiation. There is not a clear agreement of tha values of the Einstein coefficients: some values used for them can be found in [Mies 1970] or [Turnbull and Lowe 1988]. k_v^1, k_v^2 and k_v^3 represent the rate coeficients for reactions (2.25), (2.26) and (2.27). Values for k_v^1 can be found in [Lopez-Moreno et al. 1987]. The values for k_v^2 and k_v^4 are found in [Dodd et al. 1991].

For vibrational levels lower than $v = 6$, the production of excited hydroxyl is given by:

$$P(OH_v^*) = \sum_{v''>v} A_{v''v}[OH_{v''}^*] + (k_{v+1}^1[O] + k_{v+1}^2[O_2] + k_{v+1}^3[CO_2])[OH_{v+1}^*] \tag{2.29}$$

where $\sum_{v''>v} A_{v''v}$ represent production due to transitions from vibrational level v'' to a lower level v. By setting the losses from (2.28) equal to the production given by (2.29), one gets the following expression for the concentration of a given vibrational level with $v < 6$ of excited hydrogen:

$$[OH_v^*] = \frac{\sum_{v''>v} A_{v''v}[OH_{v''}^*] + (k_{v+1}^1[O] + k_{v+1}^2[O_2] + k_{v+1}^3[CO_2])[OH_{v+1}^*]}{\sum_{v'<v} A_{vv'} + k_v^1[O] + k_v^2[O_2] + k_v^3[CO_2]} \tag{2.30}$$

Expression (2.30) is a complex expression. Not only do the concentration of O, O_2 and CO_2 vary on both long and short timesclaes, the rate coefficients

are also strongly temperature dependent and will require a solid model with good input parameters to give accurate estimates of the different vibrational levels of excited hydrogen. Such a model is not used in this thesis. Therefore the most important aspect of the expression is the fact that the concentration of hydroxyl with $v < 6$ is proportional to excited hydroxyl with $v > 6$. These levels are proportional to the concentration of atomic oxygen, which in turn make all vibrational levels of atomic oxygen, including $v = 4$ and $v = 3$ proportional to the concentration of atomic oxygen.

2.4 Temperature estimates from the intensity measurements

The kinetic temperature of the mesosphere can be derived from the rotational distribution of OH*. The initial reaction (2.1) produces highly excited rotational states which do not have a Boltzman-distribution. However OH* has a relatively long radiative lifetime. Therefore the molecule will, on average, undergo at least 10 collisions [Sivjee 1991] before emitting a photon. Thus OH* will be in thermal equlibrium with the surronding mesosphere. The dirstribution of the rotational lines will be given by a Boltzmann distribution, giving rise to a intensity of each rotational line that can be expressed as follows:

$$I(v', v'', J', J) = A(v', v, J', J)C(v', J')(2J' + 1)e^{-E(v',J')kT} \tag{2.31}$$

$A(v', v'', J', J)$ are the Einstein coefficients used for a spontaneous emission from a given rotational and vibrational state to another. The coefficients found in [Mies 1970]are used to find the temperature values used in this thesis. $C(v', J')$ is the total population of the v' state. From equation (2.31) it is clear that the intensity of each rotational line is determined by two unknown quanteties, namly the temperature, T and the population of the v' state, $C(v', J')$. There excists many rotational lines, which can be observed separately. Thus the system is overdetermined and a least-square technique can be used to fit the two unknowns. In this way, measurements of the intensity of the OH Meinel (4,1) and (3,1) bands can be used to give an estimate of the temperature of the atmospere at the OH-layer.

The data used in this thesis were obtained by using a scanning Michelson interferometer manufactered by Bomen corporation placed in Antartica at the British Antarctic Survey station at Rothera (68°S, 68°W). The instrument has been used to scan the spectral region between 1000 nm and 1700 nm at about 0,5 nm resolution in the upper mesosphere. Each scan gives rise to a pattern called an interferogram. Such interferograms were scanned

rapidly and then summed to give an individual spectrum, each with an integration time of about 5 minutes. These interferograms were then Fourier transformed into spectra. A synthetic spectrum was created for each spectral position, i, by weighting the spectral contribution of each rotational line at point J, by the unit area line function of the instrument. Thus, the model at each point i is given by:

$$I_i = C(v', J') \sum_{J'} w_{i,J'} A(v', v, J', J)(2J' + 1) e^{-E(v',J')kT} \tag{2.32}$$

where $w_{i',J'}$ is the line shape weighting function. Because The Einstein coefficients and energy are known, a model syntetic spectra can be created at each data point with initial estimates of T and $C(v', J')$. Differnces between the measured spectra D_i and model spectra, I_i are equated to changes in the temperature and population via the Jacobians:

$$D_i - I_i = \frac{\partial I_i}{\partial T} dT + \frac{\partial I_i}{\partial C(v', J')} dC(v', J') \tag{2.33}$$

Then equation (2.33) results in a set of individual equations for each datapoint and dT and $dC(v', J')$ are calculated by least-square fitting and give corrections to the a prori estimates of the temperature and intensity. This process is repeated until the best fit is observed and this represents the integral band radiance and temperature of the band. The process is preformed on the spectral region of the OH Meinel (4,2) and (3,1) bands separately, and results in two independent estimates of the atmospheric temperature aswell as the integrated band radiance of each of the bands.

3 Analysis and results

The purpose of the analysis done in this thesis is to determine how the OH radiance and temperature varies on timescales of solar cycle, seasonal periods of the year and throughout the night. In this chapter the format of the data and the methods used to find the variantion in the data will be presented along with the results obtained.

3.1 Data

The data used are as described in section 2.4 obtained by a scanning Michelson interferometer placed at the British Antarctic Survey station at Rothera (68°S, 68°W). Data extending from 2002 to 2009 for both the OH Meinel (3,1) and OH Meinel (4,2) bands are used. Values for the radiance, measured in kR, along with its estimated uncertainty are collected by the method described in chapter 2.4. Values of the temperature, measured in Kelvin, are then obtained as described in the same chapter, also with an estimated uncertainty. For those unfamiliar with the unit Rayleigh(R), the unit Rayleigh is dependent on the wavelength of the photons measured and the number of photons striking a unit area. For the OH Meinel (4,2) band, 1 R will have the following connection to watts:

$$1R = 0.999 \cdot 10^{-12} \frac{\mathrm{W}}{\mathrm{m}^2 \cdot \mathrm{sr}} \tag{3.1}$$

The (3,1) band has a slightly different connection:

$$1R = 1.05 \cdot 10^{-12} \frac{\mathrm{W}}{\mathrm{m}^2 \cdot \mathrm{sr}} \tag{3.2}$$

For each night a number of individual measurements of the temperature and radiance of the OH Meinel (4,2) and (3,1) bands are made. Each such measurement is marked by the day of year and time of day it is from. Clouds may block the radiation and make the measurements unsuitable. Furthermore, when the Sun is up, sunlight with the same frequency as the OH Meinel (4,2) and (3,1) bands will be present, making measurements of the OH* radiance impossible. The Sun will also cause much smaller concentration of ozone due to photolysis [Marsh et al. 2006] through reaction (2.6). Then (2.2) indicates that the OH* concentration is also much smaller. Therefore measurements are only taken when the Sun is down. At the instruments location in Antarctica, the Sun will stay up all day during the summer. Consequently there is a large gap in the data for each Antarctic summer. In addition there are also days without measurements due to cloudy weather

and general downtime of the instrument. Some of the nights with measurements only have a very small number of individual measurements for each night. If one looks at all of the data, the variability is very large making it difficult to characterize systematic variation. This behaviour is shown in figure 3.1. In order to observe the systematic variation of the longer timescales, the

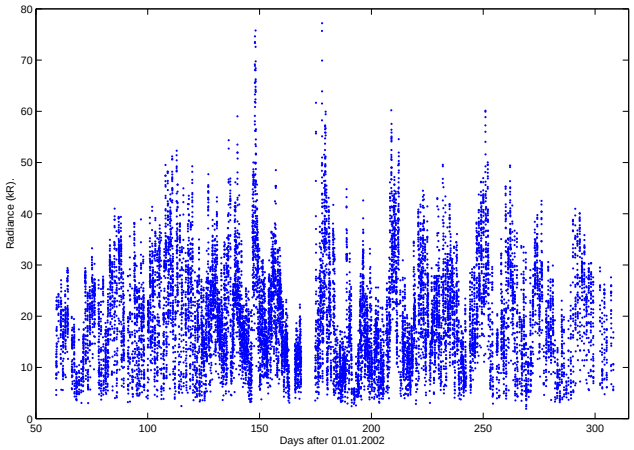

Figure 3.1: All the individual measurements for the OH Meinel (3,1) band radiance in 2002.

variation on shorter timescales must be removed. The temperature and radiance have a random variance consisting of random, statistical uncorrelated fluctuations and variations such as gravity waves and tidal oscillations with periods shorter than one day. In addition there are photochemical effects [Lowe et al. 1996, Mulligan et al. 1994]. These variations can be considered to be "'geophysical noise" since they create additional variations that can disguise longer trends. However since these variations are less than one day, averaging over the course of the night will remove these making it easier to characterize the variability on time scales longer than one day. The process used to determine the long time trends will be described in chapter 3.2. Different techniques will be used to characterize the variability during the course of a night, and how these variations change during the year. The techniques and processes used to characterize the nightly variation will be discussed in chapter 3.3. Finally chapter 3.4 will investigate the if the variations in temperature and radiance are connected.

3.2 Long trend variations

This chapter will describe the methods used to find the long time variations in the data set. Further the results obtained for the long time variation will be presented.

3.2.1 Average night

During a single night the radiance can vary by as much as a factor of three due to both photochemical and tidal effects [Lowe et al. 1996, Mulligan et al. 1994]. Also the temperature varies during the course of a night, but not by the same amount. Typical variation in the temperature during a night is around 3-5%. An illustration of variations in the radiance during a random night is given in figure 3.2. In order to filter this nightly variation from the data, all

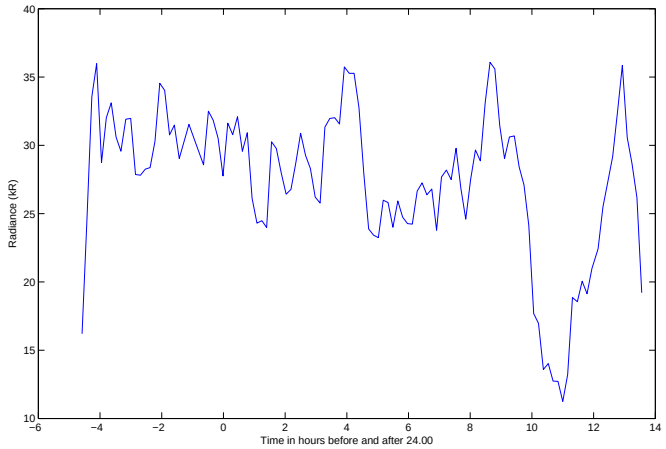

Figure 3.2: Typical variation in the radiance during a night. The plot is of the radiance of the OH Meinel (3,1) band in night 155 in 2002.

measurements for a given night were combined to an average nightly value. To prevent data gaps due to cloudy weather from skewing the average, only nights with more than 10 individual measurements are used. The average obtained is a weigthed one, calculated by use of the formula:

$$\langle A \rangle = \frac{\sum_{i=1}^{N} \frac{a_i}{(\delta a_i)^2}}{\sum_{i=1}^{N} \frac{1}{(\delta a_i)^2}} \tag{3.3}$$

Equation (3.3) is used for both the individual values for the radiation and the temperature during one night with each a_i representing one of the N measured values for the temperature or radiance for that night. δa_i represents the uncertainty of each measurement, which is estimated from the least-squares fitting procedure. The uncertainty of the average value found by equation (3.3) is calculated by the following formula:

$$\Delta A = \left(\sum_{i=1}^{N} \frac{1}{(\delta a_i)^2} \right)^{1/2} \tag{3.4}$$

Again δa_i represents the uncertainty of each of the N measurement from the night. ΔA represents the standard error of the mean. That is the value the averaged night is expected to vary from night to night.

3.2.2 Seasonal trends

After the averaging into nightly values were done, the average values for each day were put togehter to form one long data set for both the temperature and radiance of the OH Meinel (3,1) and (4,2) bands. One night is used as one unit time. Some nights are without values because they were discarded due to too few measurements. In addition, no measurements are made during the Antarctic summer. In turn this leads to sets of data with unevenly spaced gaps of different lengths. The data sets are then investigated for long time trends. Any trends in the data are assumed to be periodic. The exception is the solar cycle. Although the solar cycle does have an eleven year cycle, the data only cover the eight years from 2002 to 2009. Thus an eventual periodicity caused by the solar cycle will not go through a full cycle.

When the data are unevenly spaced and contain gaps, traditional Fast Fourier Transform analysis is not a suitable method for finding the periodic trends [Lomb 1976]. The method used for finding the significant periods in the different data sets is estimation of the power spectrum by means of the periodogram, described by [Lomb 1976] and [Scargle 1982]. Each measurement is assumed to be a combination of the actual value and random observational errors (noise):

$$X_i = X(t_i) = X_s(t_i) + R(t_i) \tag{3.5}$$

$R(t_i)$ is assumed to be statistically independent from all other $R(t_j)$ and be normally distributed with zero mean and constant variance. The periodogram, for evenly spaced data of this form, is described by:

$$P_X(\omega) = \frac{1}{N_0} \left| \sum_{j=1}^{N_0} X(t_j) \exp(-i\omega t_j) \right|^2 \tag{3.6}$$

N_0 is the number of measurements. The idea behind the periodogram is that if the data set contains a periodic(sinusoidal) component, of frequency ω_0, the factors $X(t)$ and $\exp(-i\omega t)$ will be in phase near this frequency and make a large contribution to the sum. For the other parts of the frequency the terms in the sum will be randomly positive and negative, thus yielding a small sum. Then a sinusoidal component in the data set will give a large peak in the periodogram centered around that frequency.

However [Scargle 1982] suggests a modified periodogram, better suited for unevenly spaced data. With the use of Scargle's method, P_X takes the form:

$$P_X(\omega) = \frac{1}{2}\left\{ \frac{\left[\sum_j X_j \cos(\omega(t_j-\tau))\right]^2}{\sum_j \cos^2(\omega(t_j-\tau))} + \frac{\left[\sum_j X_j \sin(\omega(t_j-\tau))\right]^2}{\sum_j \sin^2(\omega(t_j-\tau))} \right\} \quad (3.7)$$

τ is defined by.

$$\tan(2\omega\tau) = \frac{\sum_j \sin(2\omega t_j)}{\sum_j \cos(2\omega t_j)} \quad (3.8)$$

If the spacing of the data is even and has time-translation invariance, (3.7) reduces to (3.6). An example of a periodogram is shown in figure 3.3. The spectrum is obtained from data with a 0.9 Hz sinusoidal frequency. The data used to produce the periodogram is shown in figure 3.4. The data appears to be random. Nevertheless the frquency of 0.9 Hz is still clearly shown in the periodogram, illustrating the method's usefulness. A periodogram like 3.3 is often refered to as a power spectrum, and this will be done in the rest of this text. Noise in the input data of equation (3.6) can give rise to large spectral peaks which are not a result of a periodic signal. Thus it is of interest to determine the probability that a certain peak is caused by random noise. The procedure is described in [Scargle 1982]. Let $P_X = z$. For each frequency, the probabilty of finding z between z and $z + dz$ if there is no signal present at that specified frequenccy is given by:

$$p_z dz = \exp(-z) \quad (3.9)$$

The probability of finding z ,i.e. P_X, below a given value is:

$$f_z(z) = \int_0^z p_z(z')dz' = 1 - \exp(-z) \quad (3.10)$$

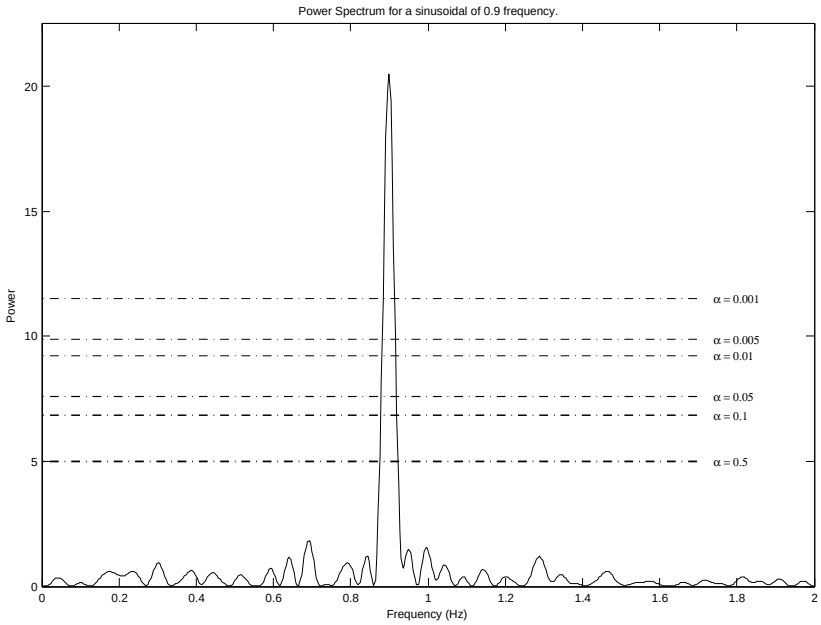

Figure 3.3: Power spectrum for data with a 0.9 Hz sinusoidal frequency

Each $P_X(\omega_n)$ is assumed to be independent. Therefore the probability of finding all N individual $P_x(\omega_n)$'s below a certain value z is:

$$F_z(x) = f_z(z)^n = (1 - \exp(z))^n \tag{3.11}$$

Thus the probability, p, of any $P_X(\omega_n)$ exceeding z, given that there are no periodic signals in the data, is:

$$p = 1 - (1 - \exp(z))^N \tag{3.12}$$

Inverting this expression to yield z as a function of p gives the following expression:

$$z = -\ln\left[1 - (1 - p)^{1/N}\right] \tag{3.13}$$

Thus if one only wants to include frequencies with less than a probability of α to be caused by random noise, one would only include frequencies with P_X equaling or exceeding a value, z_0 given by:

$$z_0 = -\ln\left[1 - (1 - \alpha)^{1/N}\right] \tag{3.14}$$

If there are significant frequencies, equation (3.14) is somewhat modified, but this effect is small when N is large. The power levels shown in figure 3.3 are

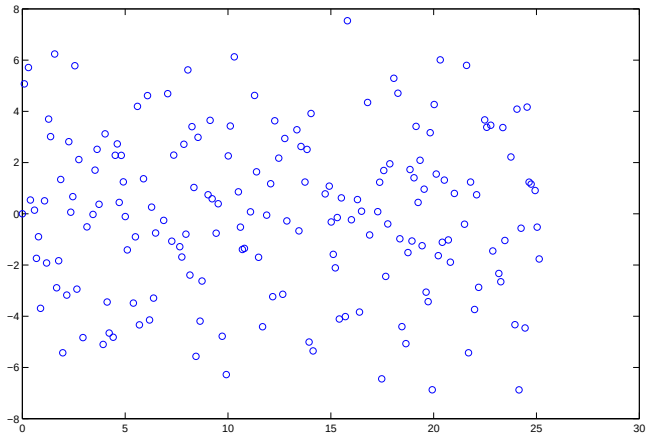

Figure 3.4: Data with a 0.9 Hz sinusoidal frequency.

obtained by the expression given in (3.14). The corresponding α-values are the probability of a frequency originating from noise exceeding the power levels, z_0. As the figure shows the power at 0.9 Hz far exceeds the $\alpha = 0.001$ level. Therefore the probability of it originating from noise is less than 0.001.

The actual analysis of the data sets were done by the procedure described in [Press and Rybicki 1988]. The long data sets were checked for statistically significant periodic signals. The resulting frequencies found in the data sets or the temperature and the radiance of the OH Meinel (3,1) and (4,2) band are summarized in table 3.1.

Radiance, (4,2)	Temperature (4,2)	Radiance (3,1)	Temperature (3,1)
(1/365)	(1/365)	(1/365)	(1/365)
(2/365)	(2/365)	(2/365)	(2/365)
(3/365)	(3/365)	(3/365)	(3/365)
-	(4/365)	-	(4/365)
-	(6/365)	-	(6/365)
(7/365)*	(7/365)	(7/365)*	(7/365)
-	(8/365)*	-	(8/365)*

Table 3.1: Significant frequencies found in the powerspectrum of the temperature and radiance data. The frequencies marked by a * are only found in the average year described in chapter 3.2.4.

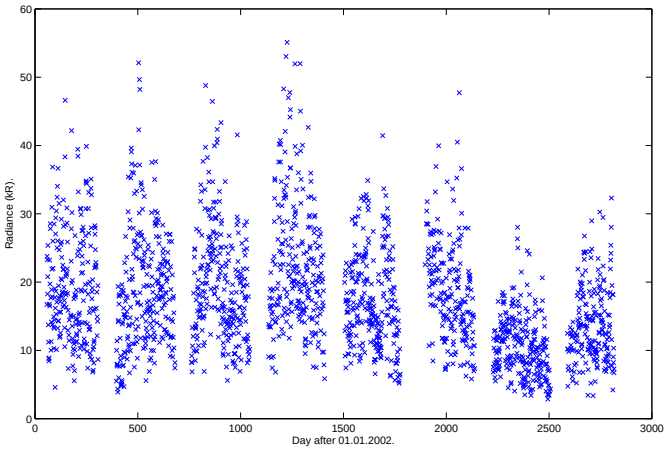

Figure 3.5: The nightly average radiance for the OH Meinel (4,2) band for all the years of measurements.

3.2.3 Solar cycle

The collected data clearly showed a reduction in the radiance and temperature towards the later years of observations. The results are easiest to spot for the radiance and is shown for the nightly average radiance of the OH Meinel (4,2) band in figure 3.5. If that reduction is a periodic one, its time period is longer than the data set. Thus Lomb-Scargle analysis is not suitable for detecting such a signal. Therefore a linear trend term is added in addition to the periodic signals in table 3.1. A very likely explanation for this reduction is the changes in solar irradiance during the solar cycle. The total solar irradiance striking the Earth's atmosphere is approximately 1367 W/m^2. However the Sun has an eleven year cycle in which the irradiance varies. These cyclic variations are to a large extent caused by magnetic activity. Reductions in the solar irradiance are caused by passage of dark sunspots across the solar disc. Increases in the radiance are due to brigth faculae. However, changes in solar irradiance during a solar cycle is no more than 0.4-0.7 W/m^2 [Solanki and Fligge 1998]. Thus the changes in total solar irradiance is not an adequate explanation for the reduction observed in the data.

However enhanced emissions in active regions above active faculae is connected to the solar cycle variation. Enhanced emission in these regions in turn leads to increasing emission of solar UV-light. Thus the intensity of high energetic UV-light will increase more than the intensity of light with longer

wavelength in periods with many brigth faculae. Thus periods with many dark spots will lead to a greater increase of high energetic light than of light with longer wavelengths, and the intensity of UV-light will vary more than the total irradiance [Lean 2005]. High energetic UV-light is responsible for the production of atomic oxygen by reaction (2.6) and the concentration of OH* is proportional to the atomic oxygen concentration. This is the reason that enhanced UV-ligh irradiance from the Sun can influence the concentration of OH*. To account for the changing UV-light from the Sun, a linear trend term is added to the periodic signals when these are fitted to the data sets. The linear trend term may be an inadequate model to represent the solar cycle variation, but is still used because the data do not extend over a full solar cycle.

3.2.4 Fits to the data

With all the parameters to be fitted to the data characterized, the fitting could be done. The frequencies found in table 3.1 were fitted to the data along with an average value and the linear trend term modeling the solar cycle. Thus the fit for the temperature/radiance took the form.

$$T(t)/R(t) = K + B \cdot t + A_1 \cos(2\pi f_1 t + \Phi_1) + A_2 \cos(2\pi f_2 t + \Phi_2) + \cdots \quad (3.15)$$

With $f_1, f_{2,\ldots}$ and $A_1, A_{2,\ldots}$ as the significant frequencies and corresponding amplitudes. $\Phi_1, \Phi_{2,\ldots}$ represents the phase of each frequency.

To find the best fit to the data, the Levenberg-Marquardt method was used. An educated guess of each parameter to be estimated is used as input along with the actual data. Let the initial guess be on the form.

$$f(t, \beta) = Y = K + B \cdot t + A_1 \cos(2\pi f_1 t + \Phi_1) + A_2 \cos(2\pi f_2 t + \Phi_2) + \cdots \quad (3.16)$$

β represents the parameters to be fitted, K, B, $A_1, A_{2,\ldots}$ and $\Phi_1, \Phi_{2,\ldots}$. Now the problem is to get model parameters β which give the best possible agreement between the model and the actual data. This is done by a least-square method, namely to minimalize the so called sum of squares.

$$\Psi = \sum_i^n = |Y_i(t) - Y(t)|^2 \quad (3.17)$$

$Y_i(t)$ represents the individual data points, $Y(t)$ the model value. New values for β are obtained in each step of the method until Ψ converges to a smallest possible value. Different methods for minimizing the sum of squares may have different disadvantages. Some models are fast, but need a good initial guess

to lead to convergence of Ψ. Others may converge even with bad guesses, but can be slow and use many iterations. The advantage of the Levenberg-Marquardt method is that it utilizes the best of two different methods. When the initial guess is far off it behaves like the method of steepest descent and can give convergence for initial guesses which would otherwise not give a solution. When β is close to the converging values, the Levenberg-Marquardt method behaves like a Taylor-series method which closes in on the converging method much faster than the method of steepest descent [Marquardt 1963].

The results obtained by this method for the OH Meinel (3,1) and (4,2) band are summraized in table 3.2 for the radiance and table 3.3 for the temperature. The frequencies found are not exactly represented by an sub-annual harmonic. But they are all so close to a sub-annual harmonic that this approximaton is used throughout the thesis. Next equation (3.3) was

	(4,2) band	(3,1) band
Average	19,58 kR	17,13 kR
Trend	1,13 kR/year	0,87 kR/year
Frequency	Amplitude	Amplitude
(1/365)	5,86 kR	3,94 kR
(2/365)	3,04 kR	2,10 kR
(3/365)	0,93 kR	0,80 kR
(7/365)*	0,78 kR	0,65 kR

Table 3.2: Fitted averages, trends and amplitudes found for the radiance. The values marked by * is for the frequencies only found in the average year.

used once more to form an average year of the temperature and radiation for the two bands. Each a_i now represents the nightly average over all years, and δa_i the standard error of the mean. N is the number of years with a value for a given day. The fit is also plotted along with the measured value. Figure 3.6 is the average year for the temperature while figure 3.7 is for the radiance. The uncertainties in the temperature values are typically more than a factor of 100 smaller than the presented value. For the radiance, the same holds for the radiance. Therefore errorbars are not included. Finally the fits were subtracted from the average year to check the average year for any remaining sub-annual frequencies. With this procedure, one additional frequency was found in each of the four data sets. A frequency of (7/365) for the radiance of the two bands. The temperature showed an additional frequency with a value of (8/365). Again the frequencies found are approximately represented by the sub-harmonics. The frequencies found only in the average year is marked by a * in table 3.1, 3.2 and 3.3.

	(4,2) band	(3,1) band
Average	183,32 K	194,76 K
Trend	0,61 K/year	0,76 K/year
Frequency	Ampiltude	Amplitude
(1/365)	32,17 K	35,75 K
(2/365)	14,13 K	15,65 K
(3/365)	2,48 K	1,79 K
(4/365)	1,93 K	1,62 K
(6/365)	0,45 K	1,44 K
(7/365)	1,77 K	2,11 K
(8/365)*	1,01 K	1,18 K

Table 3.3: Fitted averages, trends and amplitudes found for the temperature. The values marked by * is for the frequencies only found in the average year.

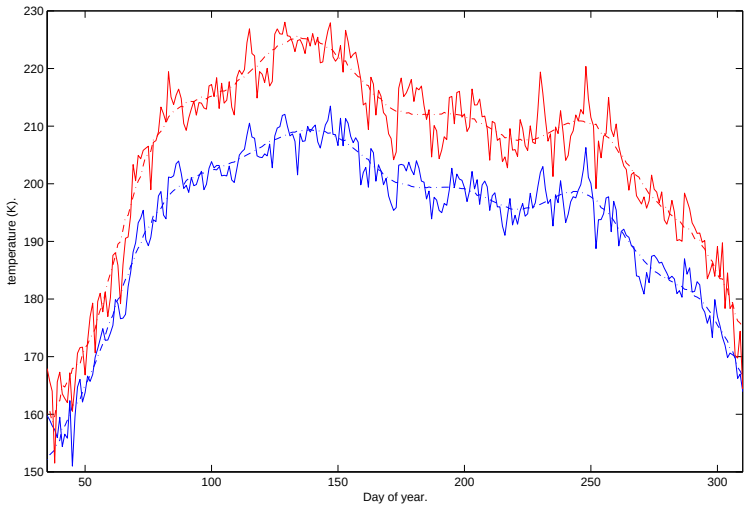

Figure 3.6: Average nightly temperature for the OH Meinel (3,1) band (red) and the OH Meinel (4,2) band (blue) for the years 2002 to 2009. The fits to the data are shown as dashed lines.

With all the frequencies, phases and amplitudes are included together with the linear trend and average value, the fit show reasonable agreement with the data. Plots of the fit together with the full data set for the OH Meinel (4,2) band are shown in figure 3.9 for the radiance and figure 3.8 for the temperature. Again the uncertainty is small compared to the presented

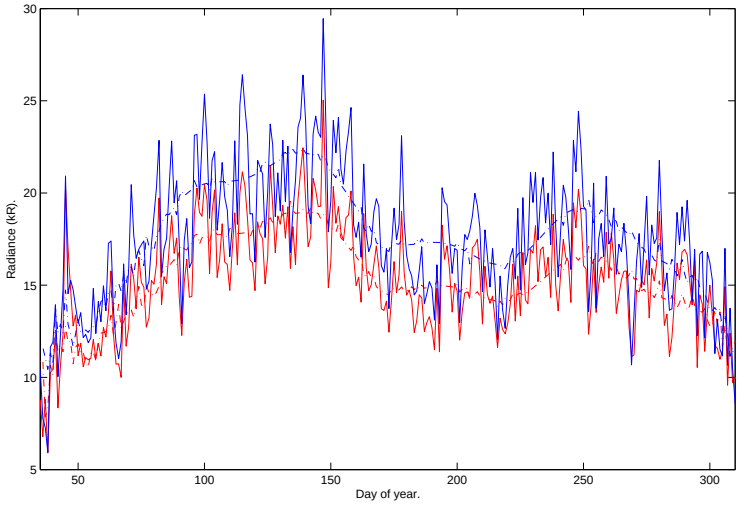

Figure 3.7: Average nightly radiance for the OH Meinel (3,1) band (red) and the OH Meinel (4,2) band (blue) for the years 2002 to 2009. The fits to the data are shown as dashed lines.

values and are therefore not included in the figure. Plots of the OH Meinel (3,1) band are found in appendix A.

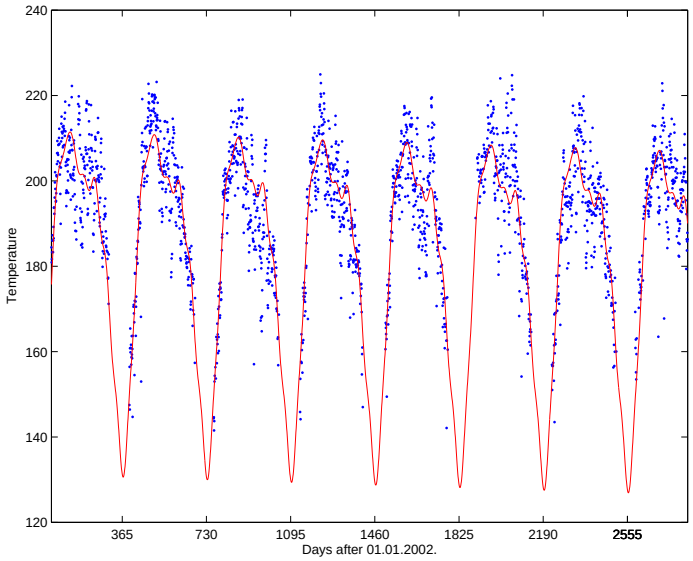

Figure 3.8: Temperature of the OH Meinel (4,2) band for 2002 to 2009. The fit to the data is shown in red.

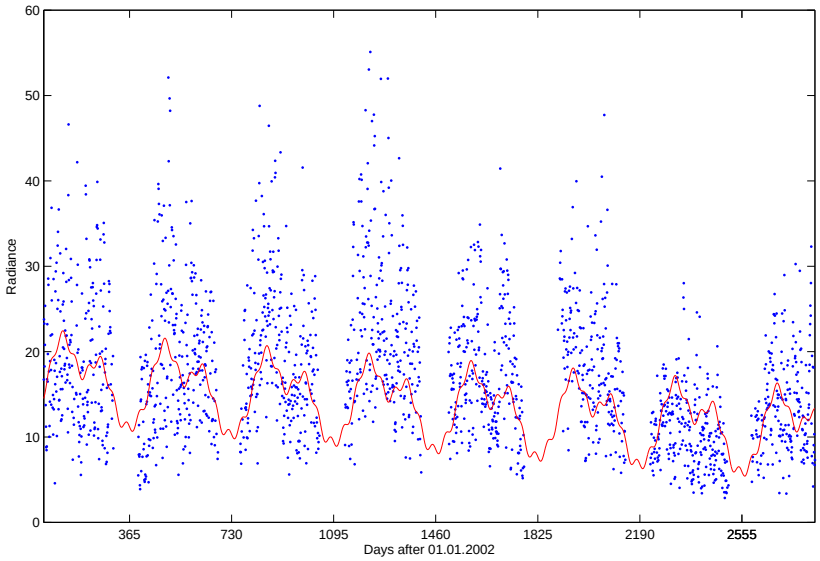

Figure 3.9: Radiance of the OH Meinel (4,2) band for 2002 to 2009. The fit to the data is shown in red.

3.2.5 Solar cycle connection

To compare the radiance and temperature with the changing solar cycle, all the model parameters obtained in the fitting given by equation (3.15) except the linear trend term, which was used to simulate a soar trend, were subtracted from the data. As an indicator of the solar cycle, the Lyman-α line of hydrogen is used. The wavelength of this line is 121.5 nm. [Pap et al. 1991] explore the possibility that the variation of the Lyman-α flux is not in complete correnspondance with the variation of total solar irradiance and the sunspot cycle. But the Lyman-α line is a good indicator for the UV-light, which is the interesting frequency domain for the production of OH*. Therefore the radiance and temperature of OH* are compared with the Lyman-α flux. The Lyman-α flux is found to vary by nearly a factor of two during a solar cycle by [Pap et al. 1991] and [Barth et al. 1990].

The Lyman-α flux used in the comparison is collected from [LISIRD 2009] (Laboratory for Atmospheric and Space Physics Interative Solar Irradiance Data Center) and is measured in units of 10^{11} photons per second per cm^2. In the rest of the thesis, this unit will be referred to as one unit La. As described in [LISIRD 2009], only model values are used in the years 2001-2003. Consequently the two first years of data are compared with model values. For the remaining years the data is compared with TIMED/SEE and SORCE/SOLSTICE observations. A scatter plot where this was plotted against the Lyman-α flux, which was used as the independent variable. To find the possible correlation between the temperature/radiance and the solar cycle variations, a linear fit of the form shown below was used.

$$T = a + b * La \tag{3.18}$$

T stands for the temperature or radiance, La for the Lyman-α flux, a and b are constants to be fitted. Plots of the temperature and radiance of the OH Meinel (4,2) band are given in figure 3.10 and figure 3.11 For both bands, the radiance and temperature showed a connection to the solar cycle. For the radiance, the (4,2) band show a stronger connection, represented y a steeper slope of the fit, than the (3,1) band. For the temperature, the situation is opposite, the (3,1) band has a steeper slope than the (4,2) band. Values for the slope obtained for the different parameters are summarized in table 3.4.

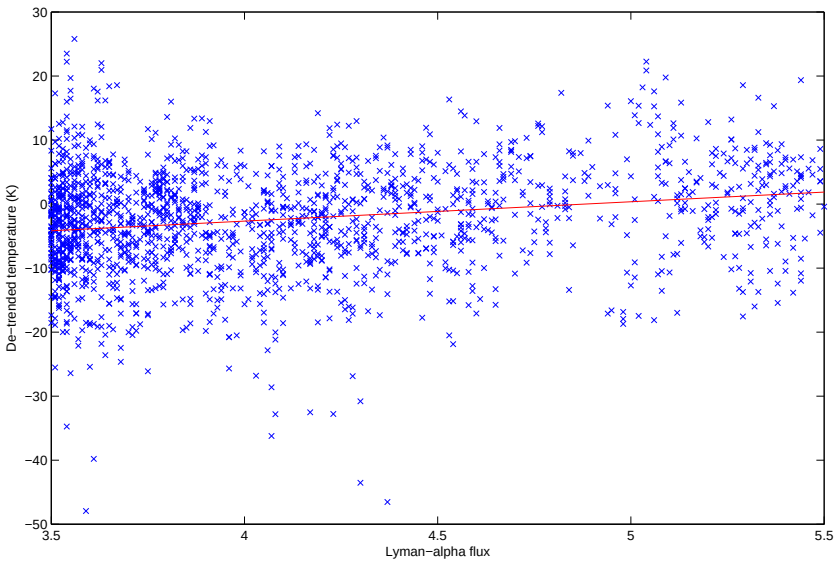

Figure 3.10: Correlation between the Lyman-α flux and temperature for the OH Meinel (4,2) band.

Temperature (4,2)	3,02 K/La
Temperature (3,1)	4,55 K/La
Radiance (4,2)	2,96 kR/La
Radiance (3,1)	2,11 kR/La

Table 3.4: Values for the slope found for the temperature and radiance.

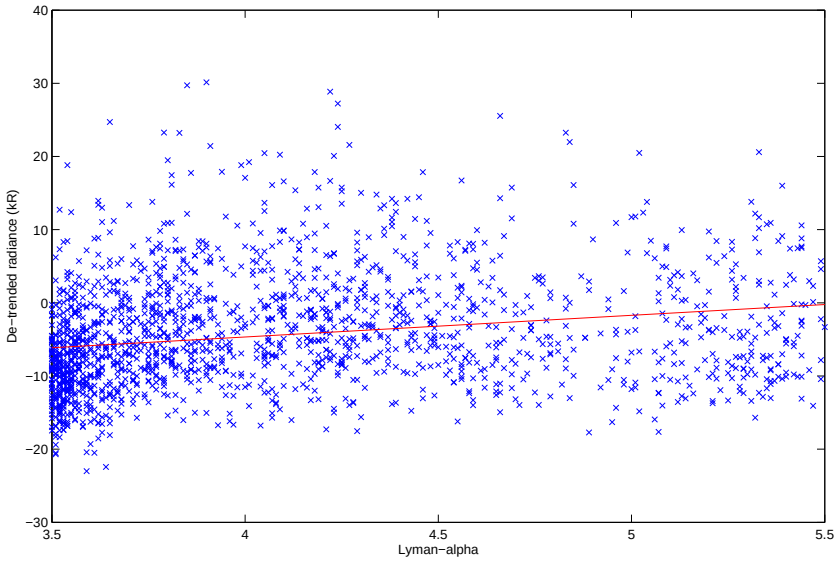

Figure 3.11: Correlation between the Lyman-α flux and radiance for the OH Meinel (4,2) band.

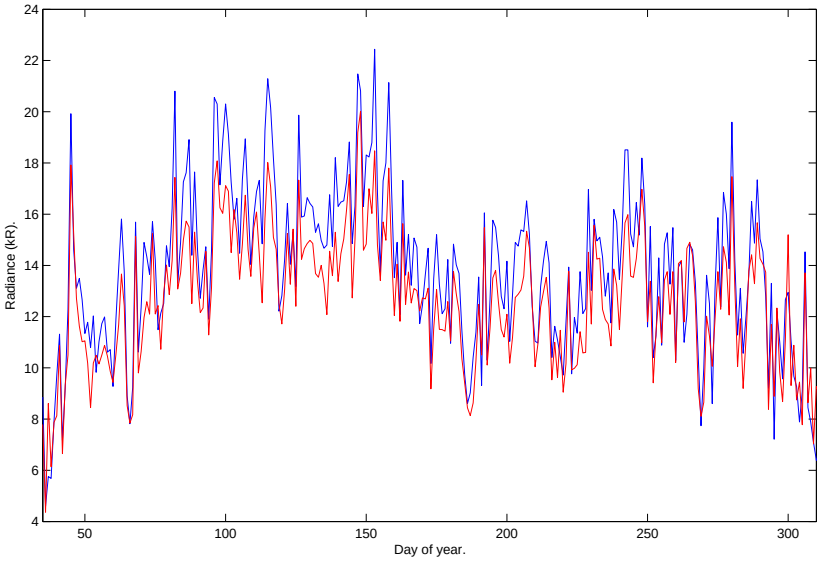

Figure 3.12: Average radiance for the OH Meinel (4,2) band (red) and (3,1) band (blue). The solar cycle variation is removed,

3.2.6 Average year

Once the connection between the solar cycle irradiance and the radiance and temperature of the two OH Meinal bands are determined, the solar variation can be removed from the data sets. With this done, an average year of all eight years can be calculated. With the solar connection removed, only the seasonal variations will be displayed in the average year. Plots of the average year is shown in figure 3.12 for the radiance and figure 3.13 for the temperature. The two largest harmonic trends for both the radiance and temperature are possible to see in the plots. The large annual variation is represented by the decreasing values found in the Antarctic summer. Also the semi-annual behaviour represented by the two peaks around equinox is is visible in the data. Further it is worth noting that the temperature of the OH Meinel (3,1) band, on average, is 11 K higher than ffor the (4,2) band. For the radiance, the situation is opposite with the (4,2) band, on average, displaying 1 kR higher values.

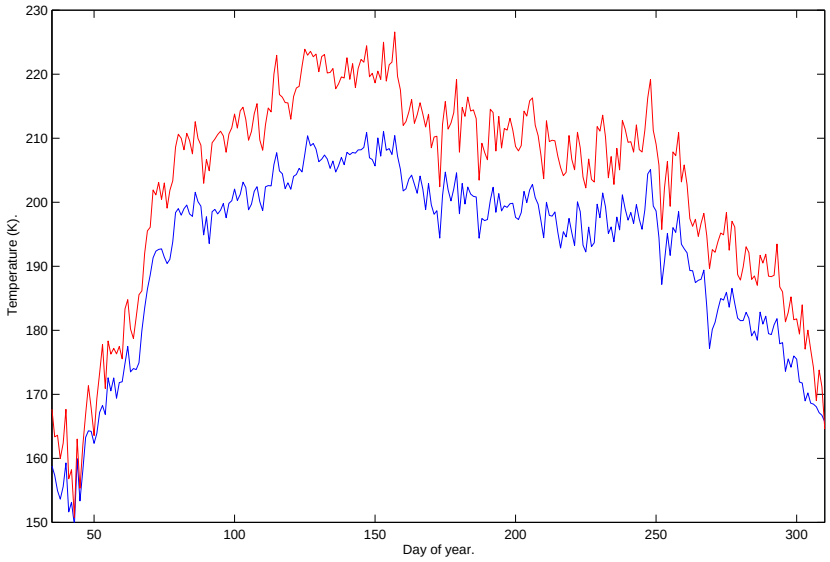

Figure 3.13: Average temperature for the OH Meinel (4,2) band (red) and (83,1) band (blue). The solar cycle variation is removed,

3.3 Diurnal variations

Once the seasonal trends are charcterized and the connection between the solar cycle and the radiance and temperature are determined. The solar cycle term can be removed from the individual data points in order to determine the diurnal variation during the year. The subtraction of these parameters will prevent the diurnal variation to be skewed by the long time variations. To find the diurnal variation, all eight years were combined to form an average year. Unlike the former plot of the average year in chapter 3.2.4, this average year will account for the diurnal variation by binning the data as a function of time for each day. The data were treated as described in chapter 3.2.6 to find the nightly average. Two different kind of plots were made. One type showed how the temperature or radiance changes with the time of the night as the time parameter. This is described in chapter 3.3.1. The other type had time after sunset as the time parameter and is presented in chapter 3.3.2.

3.3.1 Average nightly variation

Equation (3.3) is used once more to get weighted averages of the radiance and temperature. As a time resolution for one night, the night is split into 48 half hour intervals. Individual measurements are binned in their corresponding time-interval. Then bins from the same night, but different years are combined. As an example, each measurement from 02.00 to 02.30 for day 200 of the year is binned together. Finally the weighted averages is calculated. N is, as before, the number of measured values in each bin and i represents the individual measurements. Any solar cycle trends have been removed from the data before the weighted average were calculated. This was done in the following way: The difference between the Lyman-α flux for a given day and the minimum value found between 2002 and 2009 in the data from [LISIRD 2009] were multiplied with the values found in table 3.4. Next these values were subtracted from each measurement of that night. To remove the seasonal variations, the nightly averages from the average year found in chapter 3.2.6 were subtracted from each halh-hour value of the corresponding night. With this procedure the average nightly variation of both the temperature and the radiance is obtained for each night during the year.

To see how the nightly variation changes during a year, the results were plotted in the following way. The y-axis represents the time, i.e. what time of the night the value represents. The x-axis corresponds to which night of the year the value represents. What the actual value is, is represented by a colour. In other words, the plot is a coloured contour plot. This method gives the variation with the time of night as a the time parameter for each

night in the year.

To get smoother plots, each individual value was replaced with a 5 point running mean which replaced the old values, a_i, with new ones, $a*_i$. $a*_i$ were calculated in the following way.

$$a*_i = \frac{a_{i-2} + a_{i-1} + a_i + a_{i+1} + a_{i+2}}{5} \tag{3.19}$$

Different values of i corresponds to different nights. A 5 point running mean was used on all the data sets. The average diurnal variation for the temperature and radiance of the OH Meinel (4,2) band is shown in figure 3.14 and figure 3.15. Plots for the (3,1) band is found in appendix A.

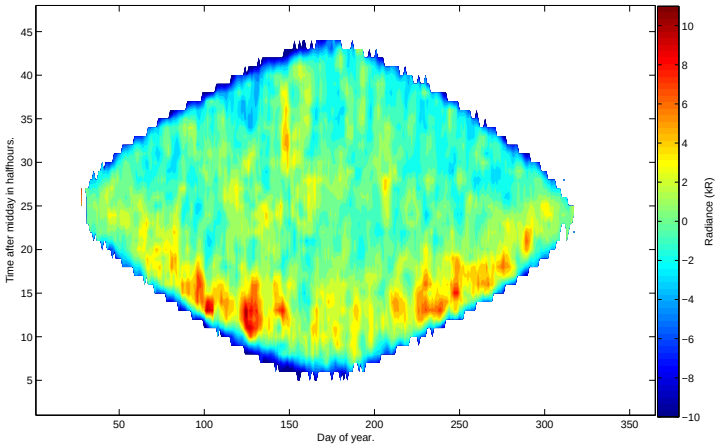

Figure 3.14: Development of the average radiance in time after sunset during a night through a year for the OH Meinel (4,2) band.

3.3.2 Average nightly variation in time after sunset

The Sun is the cause of the atomic oxygen in the mesosphere through reaction (2.6). Therefore it is perhaps of greater interest to see how the temperature and radiance varies with time after sunset. Since sunlight is the mechanism producing atomic oxygen, the time of interest is not when the Sun sets at the ground, but when the Sun sets at the OH-layer at approximately 87 km. The night is again divided into half hour intervals, but instead of using the time of the night as a parameter for binning the measurements, the time after sunset at approximately 87 km is used as a timescale. Hence all measurements made

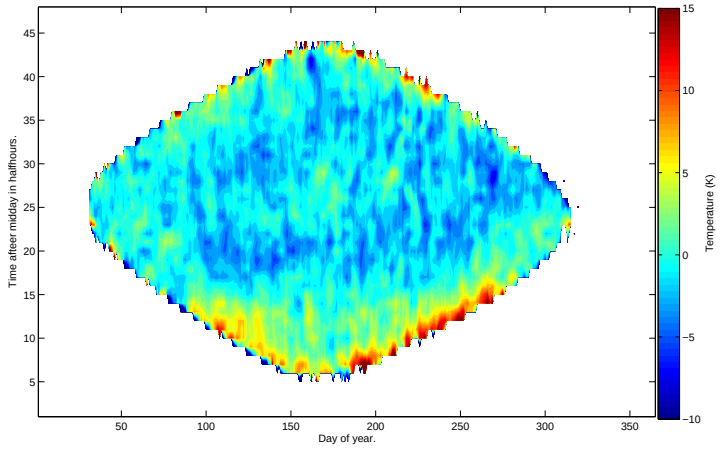

Figure 3.15: Development of the average temperature in time after sunset during a night through a year for the OH Meinel (4,2) band.

in the first half hour after sunset is binned together and so on. Next, the values for same the night of different years sre binned together to form an average night by using (3.3). As before the solar cycle trend was removed, and the values for the average year found in chapter 3.2.6 were subtracted. Plotting the reults is done in the same manner as before, with the only difference beeing that the y-axis now represents the time after sunset instead of the time of the day. Plots of the variation with time after sunset as a time parameter

Plots of the variation in the radiance of the OH Meinel (4,2) band are presented in figure 3.16, the temperature plot is displayed in figure 3.17. Corresponding plots for the OH Meinel (3,1) band are found in appendix A. At first glance, the most striking feature for both the temperature and radiance is the higher values found just after sunset. higher temperatures mean that high-lying rotational levels, far from the band center, will be brighter. Thus, these results indicate that not only will the band be brighter just after sunset, but it will also extend over a wider wave length range.

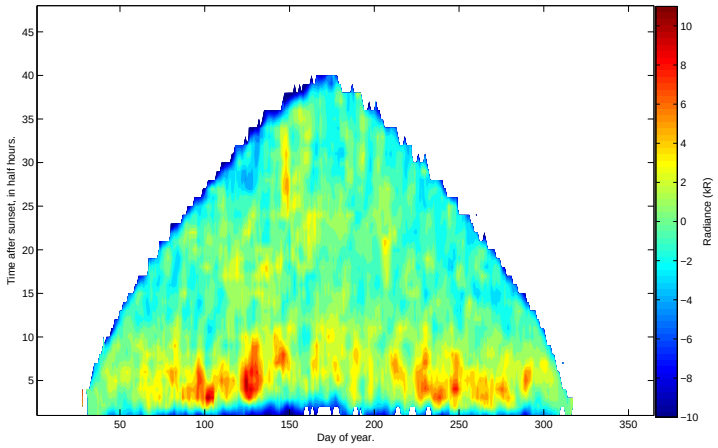

Figure 3.16: Development of the average radiance in time after sunset during a night through a year for the OH Meinel (4,2) band.

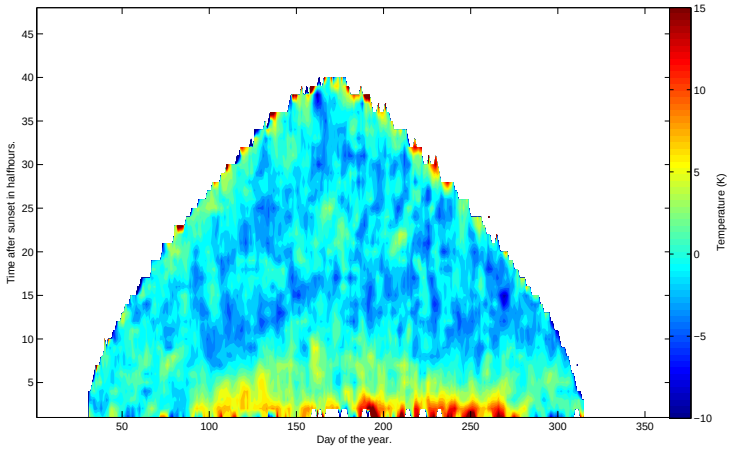

Figure 3.17: Development of the average temperature in time after sunset during a night through a year for the OH Meinel (4,2) band.

3.4 Correlations between the temperature and radiance

[Cho and Sheperd 2006] and [Espy et al. 2007] describe a correlation between the volume emmission rate(radiance) and temperature of the OH (6,2) Meinel band. Similiar correlations are found by [Cho and Sheperd 2006] during four winters ranging from 2001 to 2005. The correlation found here holds for both 15 minutes average values and averages during a full night. It is suggested in this paper that such correlations are a result of vertical motions in the mesosphere. Even though the relationship between the radiance and temperature has no influence on the long time trends, it woud be interesting to examine if such a connection appear in the data from Rothera. As shown in figure 2.1, the atmospheric temperature is approximately at a minimum at the same height as the OH* layer, 87 km. Thus downward motion will bring in warmer air. As described in subsection 2.4, the temperature estimates obtained from the intensity measurements are a good indicator of the kinetic temperature. Thus an increase in kinetic temperature will lead to an increase in the temperature obtained from the OH* emissions. Downward motions will also bring in air rich in atomic oxygen. From equation (2.5), the production rate and thus the radiance of OH* is proportional to the atomic oxygen production. For these reasons, the temperature and radiance are believed to be correlated. Reduction is believed to occur with upward motion which gives the opposite reactions. [Cho and Sheperd 2006] suggest that during the winter, all scales of variation of the temperature and radiance are caused by vertical motion. This would in turn imply that the source concentrations of atomic oxygen are constant.

[Espy et al. 2007] look at the correlation between radiance and temperature of the OH Meinel (3,1) band. Here data are presented for the whole year. The correlations between temperature and radiance are present during both summer and winter and are, as found by [Cho and Sheperd 2006], constant from year to year. However the correlation is found to be smaller in the summer time than in the the winter. A suggested explanation is that although the short-scale variations are caused by vertical motion, seasonal variations may also be influenced by changes in the atomic oxygen source function. In any case, vertical motion is believed to be the main cause of the correlation between the radiance and temperature of the OH* emissions. To see if the same correlations are found in the OH Meinel (4,2) and (3,1) bands obtained at Rothera, a scatter plot of the nightly averages obtained with equation (3.3) of temperature was plotted against the nightly averaged radiance. Next a linear trend of the form of equation (3.18) was fitted to the data to give the slope of an possible correlation. Both the temperature and ra-

diance measurements have an uncertainty. As mentioned in [Bohonak 2004] reduced major axis regression(RMA) is needed when the independent variable, say x of a fit is measured with an error. However, as a rule of thumb, RMA is not needed unless the error rate in x exceeds one third of the error rate in y. In both the OH Meinel (4,2) and (3,1) bands, the error in the radiance were considerably smaller than the error rate of the temperature. Therefore the radiance were plotted as the independent variable along the x-axis and ordinarly least square regression was used to obtain the fit. A plot for the OH Meinel (4,2) band is presented in figure 3.18. Both bands display

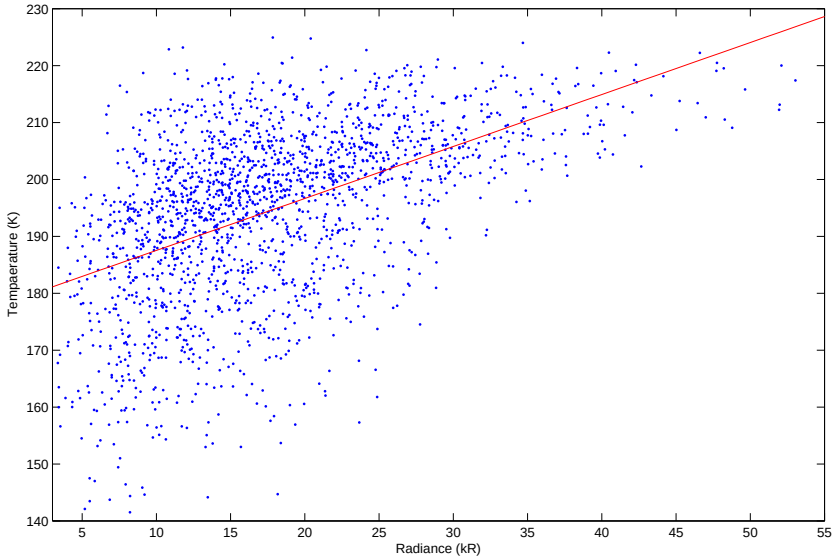

Figure 3.18: Temperature of the (4,2) band is plotted at against the radiance of the same band.

a relationship between the radiance and temperature. The connection for the two bands are given in table 3.5.

(4,2) band	(3,1) band
0.91 K/kR	1.13 K/kR

Table 3.5: correlation between the radiance and temperature for the OH (4,2) and OH (3,1) Meinel bands.

4 Discussion

The results obtained in the thesis show some distinct trends. Some of the results are in good agreement with what is found in other sudies of the OH airglow emission and temperature. An examples of this is the strong summer minima in both the temperature and radiance. Other features, like the the relatively large temperature difference between the temperature of the two bands, were not expected. In this chapter the underlying processes responsible for the most important results will be discussed. Further the different behaviour of the OH Meinel (4,2) and (3,1) bands in their connection to the solar cycle and between the temperature and radiance will be investigated. Also the connection between the radiance and temperature variation will be looked at. Finally the ideal periods for astrophysical observations determined by minimal values for the radiance will be presented.

4.1 Seasonal variations in the radiance and temperature

Here the two main seasonal trends in the radiance and the temperature, the annual and semi-annual cycles, will be presented.

4.1.1 Annual cycle

It is seen from figure 3.12 that the radiance for the two OH Meinel bands have an annual variation with a minimum in the summer. This annual behaviour with a summer minima is even clearer in the temperature and is apparent for both bands. The behviour can be seen in figure 3.13. An explanation of this annual cycle is the difference between the summer and winter hemispheres. The summer polar stratosphere will heat up more when exposed to 24 hour daylight than the winter pole which has no sunlight. Thus the summer pole will have high pressure and high temperature while the winter pole will have low temperatures and low pressure in the stratosphere. The pressure difference will give rise to a thermal wind from the summer pole to the winter pole.

When exposed to the corriolis force, this thermal wind will be bent into zonal winds by the corriolis force. In the summer hemisphere the zonal winds will be westward, in the winter hemisphere they will be eastward. [Espy and Stegman 2002], [Garcia and Solomon 1985] and [Le Texier et al. 1987] describe gravity waves originating in the troposphere with maximum amplitude at midlatitude and decreasing amplitude towards the poles. Westward

gravity waves will be stopped by the westward zonal winds when the windspeed equals the phase speed of the waves. Eastward gravity waves will be stopped by the eastward zonal winds. Thus only eastward waves will be able to penetrate the zonal winds in the summer hemisphere and only westward winds will penetrate the zonal winds in the winter mesosphere. Thus only eastward gravity waves reach altitudes where they can break and deposit their eastward momentum in the summer mesosphere. In the winter hemisphere the situation is again opposite with only westward momentum being deposited.

This will act as a drag force on the winds, causing mesopheric winds towards the equator in the summer hemisphere and away from the equator in the winter hemisphere. These meriodional winds in the mesosphere lead to downward motion at the winter pole and upward motion at the summer pole. Such an meridional circulation is described by [Garcia and Solomon 1985]. Thus air rich in atomic oxygen will propagate down to the height of the OH-layer. Since the concentration of excited hydroxyl, and in turn the radiance of the OH Meinel bands, is proportional to the atomic oxygen concentration this explain the increasing radiance in the wintertime. The minima in the radiance in the summer is caused by upward motion of air poor in atomic oxygen. Even though this process competes with higher production of atomic oxygen by reaction (2.6), it is quite clear that upward motion is the dominant process. The pressure on an air parcel will drop as it rises to higher altitudes and decrease if it falls to lower altitudes. Thus adiabatic heating and cooling are responsible for the summer minima and winter maxima in the temperature. seen in figure 3.13.

4.1.2 Semi-annual cycle

The semi-annual variation is represented by the two peaks in the radiance. One peak is centered around the spring equinox. The other is centered at a time shortly after the fall equinox. Since the radiance is proportional to the atomic oxygen concentration, the peaks should be the result of increasing atomic oxygen concentration. A likely cause for the increase is again vertical motion. Around equinox the pressure and temperature differences between the poles are very small allowing both eastward and westward gravity waves to reach the mesosphere. There the waves become unstable and break. When the waves break it leads to turbulent diffusion, in turn causing vertical motion and subsequently vertical transport of warm air rich in atomic oxygen. As described by [Le Texier et al. 1987], zonal and meriodinal winds in the stratosphere can lead to breaking of the waves before they reach the mesosphere. Thus periods of the year with weak horizontal winds will have greater

diffusion and vertical motion of atomic oxygen in the mesosphere, which in turn leads to increased radiance. Worth noting is that the large value for the radiance right before day 50 is found from just one nights measurements. Therefore this large peak is may be the result of some random statistical process.

Also the temperature of the two bands displays two peaks at the equinoxes. As for the radiance these peaks are probably the result of diffusion caused by the breaking of gravity waves. When comparing the peaks in the radiance and temperature with horizontal wind profiles at Rothera made by [Hibbins et al. 2005], it is quite clear that the horizontal winds are almost non existing at the time of the two peaks. Therefore the two peaks are expected to appear. Peaks in the radiance at the equinoxes are also found in studies of hydroxyl airglow at other locations. One example of this is at Stockholm (59 °N, 18 °E) by [Espy and Stegman 2002].

Other sub-harmonic ferquencies than the semi-annual are also found in the data for both the temperature and the radiance. One explanation of these frequencies is that the variations in the zonal winds are not strictly periodic. And even if they were, the connection between the radiance and temperature and the zonal winds is not necessarily linear. Therefore more than the annual and semi-annual periods might appear in the seasonal variations of the radiance and temperature. In addition to this effect, tidal motions with a 24, a 12 and an 8 hour period have been observed at Rothera by [Hibbins et al. 2006]. Such tidal motions along with planetary waves might also cause additional sub-harmonic frequencies in the temparature and radiance.

4.2 Solar cycle

Earlier studies have found a connection between both the mesospheric temperature, [Mohanakumar 1987] and the solar cycle and the hydroxyl airglow and the solar cycle, [Espy and Stegman 2002]. This connection is also found in the data from Rothera and will be looked at in chapter 4.2.1 for the radiance and in chapter 4.2.2 for the temperature.

4.2.1 Radiance dependency on the solar cycle

In chapter 3.2.3 the connection between the radiance and the solar cycle is investigated. The results are found in table 3.4. The OH Meinel (3,1) band display a connection of 2.11 kR/La and the (4,2) band has a connection of 2,96 kR/La. As described in chapter 3.2.3 the UV-flux will change considerably more during a solar cycle than the total irradiance. In turn these changes in the UV-flux, here represented by the Lyman-α line, will lead to changes in

the concentration of atomic oxygen. The behaviour found in chapter 3.2.6, with the (4,1) band having a stronger radiance than the (3,1) band, can give an indication as to why the connection is strongest for the (4,2) band.

Equation (2.30) gives the concentration of the different levels of vibrationally excited OH with $v < 6$. The expression shows that the concentration of $OH(v = 3)$ and $OH(v = 4)$ and in turn the radiance of the OH Meinel (4,2) and (3,1) bands is proportional to the atomic oxygen concentration. This has been discussed earllier in the thesis. Expression (2.30) is complicated and dependent on many parameters, most of them temperature dependent. Thus a good model with solid input parameters is needed to induce how the two bands radiance should change with changing atomic oxygen concentration. This is not done here, but the fact that the (4,2) band has a stronger dependence on solar cycle than the (3,1) band indicates that a certain change in the atomic oxygen concentration will lead to greatest changes for the (4,2) band.

If the connection between the radiance and solar cycle is due to changes in the atomic oxygen concentration, it is therefore not unexpected that the OH Meinel (4,2) band show the greatest connection. Both bands have increasing values for the radiance with increasing Lyman-α flux. This result is a strong indicator that the concentration of atomic oxygen is dependent on the UV-light from the Sun.

4.2.2 Temperature dependency on the solar cycle

When changes in the atomic oxygen concentration are caused by vertical motion, the temperature and radiance of the two bands will follow the same pattern. Here vertical motion is not the cause and cannot account for the connection between the temperature and Lyman-α flux. Still a strong connection between the mesospheric temperature and the solar cycle has been detected by, among others, [Mohanakumar 1987]. Here the number of sunspots is used as an indicator of the solar activity. An explanation of the connection is the increasing Lyman-α flux and its influence on the physio-chemical processes in the mesosphere which in turn influence the vertical temperature structure. [Pertsev and Perminov 2007] have also found a connection between increasing solar activity and mesospheric temperature and describe changes in horizontal winds, that affect the vertical transport in the mesosphere as the most likely cause for the connection.

Measurements of the temperature have been carried out at the same latitude as Rothera, namely at 68 °S, at Molodezhnaya. The solar-cycle connection is found to be largest at around 65 kilometers height. The connection decreases sharply with increasing height and disappears below the hydroxyl

layer, situated at around 87 kilometers. Such a result is in contrast to what is found in chapter 3.2.3 where both OH Meinel bands show a connection between the solar cycle and temperature. The (4,2) band has a connection of of 3,02 K/La and the (3,1) band have a connection of 4,55 K/La. As mentioned the connection between the temperature and solar cycle is found to decrease sharply with height. [Mohanakumar 1987] finds the connection to disappear at around 75 kilometers.

Hydroxyl in different vibrational states are not necessarily situated at the same altitude. [Lopez-Moreno et al. 1987] describe a difference in the peak of $OH(v = 3)$ and $OH(v = 4)$ at (37 °N, 6 °W) with $OH(v = 4)$ having its peak at 90 kilometers, 5 kilometer above the peak of $OH(v = 3)$ at 85 kilometers. The MSIS model also predicts and altitude difference, although a smaller one of around 1 kilometer. If the connection exhibits roughly the same vertical profile at Rothera as it does at Molodezhnaya, it may explain the difference between the two bands. This is because the of the sharp decrease in the connection with height. Therefore the height difference would be expected to lead to a stronger connection between the Lyman-α flux and temperature for the (3,1) band, which also is found. Thus the connection between the solar cycle and temperature probably follow the same pattern at Rothera as at Molodezhnaya, but extend further up in the atmosphere. Other studies, like [Pertsev and Perminov 2007], also find the connection to extend up to the mesosphere.

4.3 Diurnal variation

After sunset there will be no sunlight present to produce atomic oxygen. Thus the concentration of atomic oxygen will decrease due to chemical reactions like reaction (2.3). The production of excited hydroxyl is as shown in equation (2.5) proportional to the concentration of atomic oxygen. Excited hydroxyl will radiate and cascade down to lower vibrational states until the lowest level is reached. The concentration of the lower levels and in turn the radiance of the OH Meinel (4,2) and (3,1) bands is given by equation (2.30) and is proportional to the atomic oxygen concentration. Since no more atomic oxygen is produced after sunset, this concentration, and in turn the radiance, should show a contionious decrease throughout the night. [Lowe et al. 1996] describes an exponentional reduction in the atomic oxygen concentration, with a time constant, τ, given by:

$$\tau = \frac{1}{k_{O+O_2+M}[O_2][M]} \tag{4.1}$$

The time parameter is time after sunset. From equation (4.1), it is seen that larger concentrations of atomic oxygen will lead to a longer survival time of the atomic oxygen. Since the concentration of atomic oxygen increases with height [Melo et al. 2001] at altitudes below the hydroxyl layer, the lifetime of atomic oxygen will increase with height beyond a certain height, usually taken to be around 86 km [Lowe et al. 1996], where the lifetime exceeds 24 hours.

If only chemical reactions described by (2.3) and (2.2) were responsible for the changing concentration of atomic oxygen and ultimately the radiation from the OH Meinel (4,2) and (3,1) bands, this radiation should show a continious decrease throughout the night. [Lowe et al. 1996] finds that the values for τ for different heights from measurements disagrees with the ones calculated assuming only chemical decay of atomic oxygen in the latitude range of 35°to 45°. Indications that there are more than chemical processes responsible for the changes in radiance during the night is also found in this thesis. Figure 3.14 and to an even greater degree figure 3.16 show that the radiation of the OH Meinel (4,2) band do not show a contionious decrease in time after sunset. Even though the radiance decreases from the values displayed a short time after sunset, some of the nights show approximately constant radiance. Others even display increasing radiance at the end of the night. With an exponential decay through the night, a logaritmic plot of the radiance should have a linear decrease throug the night. All the days of the year have been averaged into one average night, then the natural logarithm of the radiance were taken and plotted against the time after sunset to get a more concrete way to examine if chemical decay is the only contributing process or not. The plot is shown in figure 4.1. From the plot it is quite clear that more than chemical processes contribute to the decay of atomic oxygen at the height of the hydroxyl layer.

[Lowe et al. 1996] list two probable causes for the difference between the measured and calculated time constants. Either that a process faster than (2.3) controls the atomic oxygen or that vertical motion lead to changes in the concentration. Since figure 4.1 does not show a continious decrease through the night, the second explanation involving vertical motion is the most likely. If this vertical motion displays seasonal variations, these variations can explain the changing pattern of the nightly radiance during the year.

[Espy and Stegman 2002] use the CIRA-86 wind model to generate values for the diffusion at 60 °N and find the values for diffusion at heigths above 90 kilometers to be largest around the equinoxes with minima in the summer and the winter. Behaviour of the same kind can be seen in the data from Rothera (68 °S). A continious decrease throughout the night is not clearly

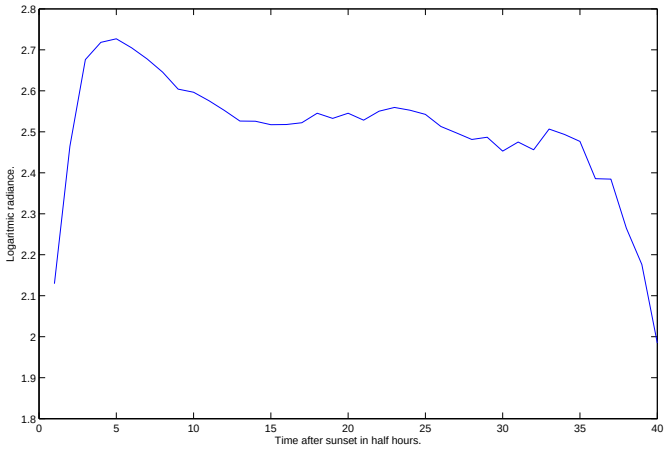

Figure 4.1: Average nightly variation of the radiance of the OH Meinel 84,2) band through the night on a logaritmic scale.

present at any time during the year. Around day 150, figure 3.16 show that the radiance increases towards the end of the night, indicating stronger vertical transport of atomic oxygen. In chapter 4.1.2 the large values found for the radiance around day 150 is explained by the weak zonal winds at that time of year allowing gravity waves to break and cause vertical diffusion at the hydroxyl layer. That the greatest diurnal variance and greatest absolute value of the radiance occur at the same time of year strengthens the suggestion that vertical motion caused by breaking gravity waves is the origin of these features. However, the decrease in radiance is not continious at any time during the year. Thus tidal motions and planetary waves like the ones descrbed in [Hibbins et al. 2006] are probably responsible for further vertical motion than the diffusion caused by breaking gravity waves at the equinoxes. A plot of the radiance of the OH Meinel (3,1) band is presented in appendix A. The (3,1) band follows the same pattern as the (4,2) band.

By the reasoning used in chapter 3.4 vertical motion due to breaking gravity waves should lead to similiar changes in the temperature and the atomic oxygen concentration. Such variations are not present in figure 3.15 and figure 3.17, which show the diurnal temperature variation for the OH Meinel (4,2) band. The only clear trend is the high values found at the start of the night right after sunset. The lower values found after that time is probably due to the fact that the Sun has set. Similar behaviour is found for the temperature of the (3,1) band and plots of this band can be found

in appendix A. This indicates that the temperature at the height of the hydroxyl layer varies on a nightly basis by other mechanismes in addition to vertical motion.

4.4 Temperature differences between the OH Meinel (4,2) and (3,1) bands

Figure 3.13 shows that the temperature of the OH Meinel (3,1) band is higher than the temperature of the (4,2) band. On average the difference is 11 K. As described in chapter 2.4, the temperature of the OH Meinel bands should be close to the kinetic temperature at the emitting height. Therefore the temperature for the two bands should have roughly the same values. The temperature difference could indicate that hydroxyl in different vibrational states are located at different heights. As described in chapter 4.2.2, the MSIS model predicts an altitude difference of 1 kilometer. Further the MSIS model predicts a temperature dependence of 1,5 K/km at the height of the hydroxyl layer at Rothera in the winter. Using the results from the MSIS model can therefore not account for the temperature difference of 11 K between the bands. Thus the MSIS model indicates that the temperature difference of the two bands is not caused by height differences between the emitting layers. One likely explanation may then be calibration errors of the measuring instrument. The detector respomse falls rapidly through the (4,2) band region as compared to the relatively flat response over the (3,1) band. This makes the (4,2) band intensity, and hence the extracted temperature, sensitive to calibration errors.

In situ rocket measurements have been made by [Lübken et al. 1999] at Rothera. Here the vertical structure of the temperature was observed. In this study, the mesospause is found to be centered at around 88 kilometers. Thus $OH(v = 3)$ and $OH(v = 4)$ have peaks in the concentration around the mesospause. Consequently, the temperature for the two OH Meinel bands should have approximately the same values despite of the height difference. [Lübken et al. 1999] have only made measurements in January and February. The data used in this thesis have no values before mid February due to continious sunlight in the Antarctic summer. Further it is seen from figure 3.13 that the difference in temperature between the two bands is smallest in the summer. Therefore it is more relevant to examine the vertical temperature profile in the summertime.

No measurements have been done at Rothera for the wintertime vertical temperature profile. However, Lidar meaurements of the mesospheric temperature have been made at the South Pole covering the whole year. These

measurements are summarized by [Pan and Gardner 2003]. Here it is found that the mesospause changes in height from 88 kilometers in the summer to around 100 kilometers in the winter. Then the temperature will decrease with increasing altitude in the summer at the altitudes of the hydroxyl layer. Compared with the MSIS model, the data from the South Pole show a higher altitude of the mesospause in the winter. Further the temperature gradient is considerably steeper at the height of the hydroxyl layer. Therefore the results of [Pan and Gardner 2003] can indicate that the MSIS model do not show a steep enough temperature gradient in the wintertime at Rothera.

As shown in equation (2.30), the concentration of the different vibrational states of excited hydroxyl are temperature dependent. Thus a change in the temperature could also increase the height difference of the two states. Should calibration errors be the only cause for the differences in the measured temperatures, the difference is expected to be fairly constant throughout the whole year. There is found an increase in the difference in wintertime compared to summertime, which may also indicate that more than calibration errors could cause the difference. The peak of the $OH(v = 3)$ layer lies below the $OH(v = 4)$ peak. Thus the temperature is expected to be lower for the OH Meinel (4,2) band than for the (3,1) band in the summertime. Should the gradient at Rothera be steeper than predicted by the MSIS model combined with a greater height difference, this could account for at least some of the measured temperature difference, especially in the summertime.

4.5 Connections in the temperature and radiance variation

From the results in chapter 3.4, the OH Meinel (3,1) band show a stronger variation in the temperature for a given change in the radiance than the (4,2) band. Both bands show a connection with a value of 1,13 K/kR for the (3,1) band and 0,91 K/kR for the (4,2) band. Since air from above the layer will be rich in atomic oxygen, downward motion will increase the radiance and upward motion will bring in air with a smaller atomic oxygen concentration. As described in chapter 4.1.1, adiabatic heating of downward air parcels and adiabatic cooling of upward moving air parvels is the cause for annual changes in the temperature. Therefore the annual cycle of the temperature and radiance follow the same pattern, giving rise to a connection. The semi-annual behaviour which probably is caused by diffusion, will cause warm air rich in atomic oxygen to reach the hydroxyl layer. Therefore the semi-annual behaviour of the temperature and radiance follow the same pattern. Since the temperature and radiance follow approximately the same seasonal

pattern, the connection is not unexpected. The two bands do however show a different degree of connection between the temperature and radiance.

In chapter 4.2.1 it is explained why the OH Meinel (4,2) band is expected to vary more than the (3,1) band when exposed to the same changes in the atomic oxygen concentration. The temperature will change by approximately the same amount for both bands due to vertical motion, while the radiance will change more for the (4,2) band than for the (3,1) band. Thus the gradient, given by $\Delta T/\Delta R$, should be steeper for the (3,1) band than for the (4,2) band. The values from chapter 3.4 do agree with this reasoning, further strengthening the indications that vertical motion is the main source for changing values for the temperature and radiance in the two OH meinel bands.

4.6 Ideal observation periods

Trends in the radiance on all scales found at Rothera can give an indication of the trends at other places in Antarctica. The varying radiance can be used to define the optimal observation periods of astrophysical observations in the near infrared region of 1-2.2 μm, in particuar the H band transmission between 1,47 and 1,82 μm. The most important trends is as mentioned in chapter 4.1, 4.2.1 and 4.3 the annual and semi-annual cycle, the diurnal variation and the solar cycle variations.

Firstly the diurnal variations throughout the year displayed in figure 3.14 give one clear indication as to at what time of the night the radiance displays the largest values. The five hours after sunset are approximately 2 to 10 kR brighter compared to the time of night after this five hour period. This kind of behaviour is found throughout the whole year. Therefore it is obvious that any astronomical studies in the infrared region should be taken more than five hours after sunset if possible. The exceptions are the short days in the Antarctic spring and fall where the night is shorter than 5 hours.

The two main features of the seasonal variation in the infrared radiance of hydroxyl is the semi-annual and annual variation which can be seen in figure 3.12. The peak at fall equinox is considerably higher than the one at spring equinox. The difference between the winter minima in the radiance and the smaller spring equinox maxima makes this winter minima around day 200 the time of year best suited for astronomical observations. Another aspect making this a suitable period for observations is the long nights in the Antarctic winter. The low values observed for the radiance in the beginning and end of the Antarctic summer might at first glance indicate this to be a good time to do observations. However the night is relatively short at this time of year making these periods less suitable for observations.

Finally there is a strong connection between the solar cycle and hydroxyl radiance. Even though the correlation is stronger for the OH Meinel (4,2) band than for the OH Meinel (3,1) band, both bands show a strong correlation. The corelation arises because changes in UV-light during a solar cycle influence the concentration of atomic oxygen. Therefore all vibrational levels of OH* will vary with the solar cycle. The values for the radiance are smallest when there is little UV-light and larger when the UV flux is high. Thus the ideal periods for astronomical observations are in the solar cycle minima.

In summary, these results indcate that the following observational periods are optimal for reducing the infrared background radiance from the rotation-vibration transitions in excited hydroxyl at Antarctica. If possible astronomical observations should be done in years in which the Lyman-α flux from the Sun have small values, i.e. when the solar cycle is in a minima. Further the observations should be done at at the winter minima in the radiance. This minima is found around day 160 to day 230 of the year. Finally the observations should be done more than 5 hours after sunset to avoid the the time of night with most radiance from excited hydroxyl.

4.7 Conclusions

Ground based measurements of the hydroxyl airglow and temperature of the OH Meinel (4,2) and (3,1) bands have been made at Rothera (68 °S,68 °W) during an eight year period from 2002 to 2009. The hydroxyl airglow is the main background source for astronomical observations in the infrared and near infrared. Therefore the variations in the hydroxyl radiance were investigated. Also the temperature variations were examined as higher temperate hydroxyl will radiate over a more extensive spectral region..

Both the temperature and the radiance of the two bands were found to vary on nightly, seasonal and solar-cycle timescales. The temperature and radiance have many similarities in their variance on seasonal time scales. The main features shared by the temperature and radiance is the summer time minima and the peaks at the equinoxes. Seasonal variations are probably caused by vertical motion in the mesosphere, which give rise to roughly the same variations in the temperature and radiance. Further both the temperature and radiance showed increasing values in periods with increasing solar activity during a solar cycle. This increase is the result of increasing UV flux from the Sun. The nightly variation of the temperature and the radiance changes from day to day. However, the trend is that the highest values are found in the time right after sunset for both.

Astronomical observations in the infrared and near infrared region should be done when the background is at its lowest. From the analysis made in this study, these periods are when the solar cycle is in a minima. The time of year best suited for measurements is between the two equinox maxima, from around day 160 to day 230 of the year. Such obsevartions must be carried out during the night. The hydroxyl airglow have distinctly higher values in the first 5 hours after sunset, therefore astronomical observations should be carried out more than 5 hours sunset in order to minimize the background radiation.

References

[Andrews 2000] Andrews, D.G. An introduction to atmospheric physics, pp.9-10: New York, Cambridge Univerity Press, 2001.

[Azeem et al. 2007] Azeem S.M.I., Sivjee G.G., Won Y.I., and Mutiso C. Solar cycle signature and secular long-term trend in OH airglow temperature observations at South pole, Antarctica. *Journal of Geophysical Research,* Vol. 112, A01305, doi:10.1029/2005JA011475, 2007.

[Baker and Stair 1988] Baker D.J. and Stair J.T. Rocket measurements of the altitude distributions of the hydroxyl airglow, *Physica Scripta.,* Vol. 37, pp. 611-622, 1988.

[Barrett 2010] , Barrett Bellamy Climate. Available from: http://www.barrettbellamyclimate.com/userimages/PQRCO2.jpg [Accessed: April 11, 2010].

[Barth et al. 1990] Barth C.A., Tobiska W.K., Rottman G.J. and White O.R. Comparison of 10.7 cm radio flux with SME Solar Lyman alpha flux. *Geophysical Research Letters,* Vol. 17, No.5, pp 571-574, 1990.

[Boeker and Grondelle 2001] Boeker E. and Grondelle R., Enviromental science: Physical principles and applocations, pp.14: Chichester, John Wiley & sons Ltd., 2001.

[Bohonak 2004] Bohonak, A.J. (2004), RMA. Available from: San Diego State University, Web site: http://www.bio.sdsu.edu/pub/andy/rma.html [Accessed: April 22, 2010].

[Cho and Sheperd 2006] Cho Y.M. and Sheperd G.G., Correlation of airglowtemperature and emission rate at Resolute Bay (74.68°N), over four winters (2001-2005) *Geophysical Research Letters,* Vol. 33, L06815, doi:10.102972005GL025298, 2006.

[Content 2005] Content R. Deep-sky infrared imaging by reduction of the background light 1. Sources of the background and potenial suppresion of the OH emission. *The Astrrophysical Journal,* Vol 464, pp.412-425, 1995.

[Corbett et al. 2007] Corbett J., Butterley T. and Allington-Smith J.R. Fibre modal power distributionin astronomy and their application to Ohsuppresion fibres. *Royal Astronomical Society,* Vol. 378, pp. 482-492, 2007.

[CRISP] Center for Remote Imaging, Sensing & Processing. Available from: http://www.physics.nus.edu.sg/ crisp/cd2001/tutorial/atmos.htm [Accessed: May 4, 2010].

[Davies 2006] Davies R.I. A method to remove residual OH emissions from near infrared spectra. *Royal Astronomical Society,* Vol. 375, pp. 1099-1105, 2006.

[Dodd et al. 1991] Dodd J.A., Lipson S.J. and Blumberg W.A.M. Formation and relaxation of ($OH(X^2II-l,V)$ by O_2 and CO_2 *Journal of Chemical Physics,* Vol. 95, pp. 5798-5802, 1991.

[Ditky et al. 2010] Ditky G., Schmidt H., Weber M., von Savigny C. and Mlynczak M.G. Daytime ozone and temperature in the mesosphere: A comparison between SABER observations and Hammonia model, *Atmospheric Chemistry and Physics,* Discuss., 10 2005-2029, 2010.

[Espy et al. 2007] Espy P.J., Stegman J., Forkman P. and Murtagh D. Seasonal variation in the correlation of airglow temperature and emission rate, *Geophysical Reasearch Letters,* Vol 34, L17802, doi:10.1029/2007Gl031034,2007.

[Espy and Stegman 2002] Espy P.J. and Stegman J. Trends and variability of mesospheric temperature in high-latitudes. *Physics and Chemistry of the Earth,* Vol. 27, pp.543-553, 2002.

[Garcia and Solomon 1985] Garcia R.R. and Solomon S. The effect of breaking gravity waves on the dynamics and chemical composition of the mesosphere and lower thermosphere, *Journal of Geophysical Research,* Vol. 90, NO. D2, pp.3850-3868, 1985.

[Hemmer 2005] Hemmer, P.C. Kvantemekanikk. 5th. Ed, pp. 105: Trondheim: Tapir Akademiske Forlag, 2005.

[Herzberg 1971] Herzberg, G. The spectra and structure of simple free radicals: An introduction to molecular spectroscopy. New York: Dover Publications,inc, 1971.

[Herzberg 1950] Herzberg G. Spectra of diatomic molecules. 2nd. Ed. New York: Van Nostrand reinhold Company Inc, 1950.

[Hibbins et al. 2005] Hibbins R.E., Shanklin J.D., Espy P.J., Jarvis M.J., Riggin D.M., Fritts D.C. and Lübken D.J. Seasonal variations in the horizontal wind structure from 0-100 above Rothera station, Antarctica

(68 °S, 67 °W). *Journal of Atmospherical and Chemical Physics,* Vol. 5, pp.2973-2980, 2005.

[Hibbins et al. 2006] Hibbins R.E., Espy P.J., Jarvis M.J., Riggin D.M. and Fritts D.C. A climatology of tides and gravity wave variance in the MLT above Rothera, Antarctica obtained by MF radar. *Journal of Atmospheric and Solar-Terrestrial Physics,* Vol. 69, pp.578-588, 2006.

[Iwamuro et al. 1994] Iwamuro F., Maihara T., Oya S., Tsukamoto H., Hall D.N.B., Cowie L.L., Tokunaga A.T. and Pickles A.J. Development of an OH-airglow suppressor spectograph. *Astronical Society of Japan,* Vol. 46, pp.515-521, 1994.

[Lean 2005] Lean J., Living with a variable Sun *Physics today,* 2005.

[Le Texier et al. 1987] Le Texier H., Solomon S. and Garcia R.R. Seasonal variability of the OH meinel bands. *Planetary and Space Science,* Vol.35, No. 8, pp.977-989, 1987.

[Lomb 1976] Lomb N.R. Least-squares frequency analysis of unequally spaced data, *Astrophysics and Space Science,* Vol. 39, pp. 447-462, 1976.

[LISIRD 2009] LISIRD - Composite Lyman-alpha. Available from: University of Colorado, Laboratory for Atmospheric and Space Physics Web site: http://lasp.colorado.edu/lisird/lya/ [Accessed: February 23, 2010].

[Lopez-Moreno et al. 1987] Lopez-Moreno J.J., Rodrigo R., Moreno F., Lopez-Puertas M. and Molina A. Altitude distribution of vibrationally excited states of atmospheric hydroxyl at levels $v = 2$ to $v = 7$ *Planetary and Space Science,* Vol. 35, No 8, pp. 1029-1038, 1987.

[Lowe et al. 1996] Lowe R.P., Leblanc L.M. and Gilbert,K.L. WINDII/UARS observation of twilight behaviour of the hydroxyl airglow, at mid-latitude equinox, *Journal of Atmospheric and Terrestrial Physics*, Vol 58, No. 16, pp. 1863-1869, 1996.

[Lübken et al. 1999] Lübken F.J., Jarvis M.J. and Jones G.O.L. First in situ temperature measurements at the Antarctic summer mesospause. *Geophysical Research Letters,* Vol. 26, No. 24, pp. 3581-3584, 1999.

[Maihara et al. 1993] Maihara T., Iwamuro F., Yamashita T., Hall D.N.B., Cowie L.L. Tokunga a.T. and Pickles A. Observations of the OH airglow emission. *Astronomical Society of the Pacific,* Vol. 105, pp. 940-944, 1993.

[Marquardt 1963] Marquardt D.W., An algorithm for least-squares estimation of nonlinear parameters *Society for INdustrial and Applied Mathematics,* Vol. 11, pp. 431-441, 1963.

[Marsh et al. 2006] Marsh, D.R., Smith, A.K., Mlynczak, M.G. and Russell, J.M., SABER observation of the OH Meinel airglow near the mesopause, *Journal of Geophysical Research,111,* A10S05, doi:10.1029/2005JA011451.

[Melo et al. 2001] Melo S.m.L.,mcDade i.C. and Takahashi H. Atomic oxygen profile from ground-based nightglow measurements at 23°S. *Journal of Geophysical Research,* Vol. 106, No. D14, pp.15377-15384, 2001.

[Meinel 1950] Meinel A.B. OH emission bands in the spectrum of the night sky, II. *American Astronomical Society,* Vol. 111, pp. 555-564, 1950.

[Mies 1970] Mies F.H. Calculated vibrational transition probabilities of OH(X^2II), *Journal of Molecular Spectroscopy,* Vol. 53, pp.150-188, 1974.

[Mohanakumar 1987] Mohanakumar K., Response of an 11-year solar cycle on middle atmospheric temperature. *Physica Scripta,* Vol. 37, pp. 460-465, 1987.

[Mulligan et al. 1994] Mulligan F.J., Horgan D.F., Galligau J.G. and Griffin E.M., Mesopause temperature and integrated band brightness calculated from airglow OH emissions recorded at Maynooth (52,2 °N, 6,4 °W) during 1993. *Journal of Atmospheric and Terrestrial Physics,* Vol. 37, No. 13, pp. 1623-1637, 1995.

[Pan and Gardner 2003] Pan W. and Gardner C.S., Seasonal variation of the atmospheric temperature structure at South Pole. *Journal of Geophysical Research,* Vol. 108, No, D18, 4564, doi:10.1029/2002JD003217, 2003.

[Pap et al. 1991] Pap J.M., london J. and Rottman G.J., Variability of solar Lyman Alpha and total solar irradiance, *Astronomy and Astrophysics,* Vol. 245 pp. 648-655, 1991.

[Pertsev and Perminov 2007] Pertsev N. and Perminov V. Response of the mesopause airglow to solar activity infrared from mesurements at Zvenigorod, Russia. *Annales Geophysica,* Vol. 25, pp. 1-8, 2007.

[Press and Rybicki 1988] Press W.H. and Rybicki G.B. Fast algorithm for spectral analysis of unevenly sampled data. *The Astrophysical Journal,* 338:277-280, 1989.

[Scargle 1982] Scargle J.D. Studies in astronomical time series analysis. II. Statistical aspects of spectral analysis of unevenly spaced data *The Astrophysical Journal,* 263:835-853, 1982.

[Sivjee 1991] Sivjee G.G. Airglow hydroxyl emissions, *Planetary and Space Science,* Vol.40, No. 2/3, pp. 235-242, 1992.

[Solanki and Fligge 1998] Solanki S.K. and Fligge M., Solar irradiance since 1874 Revisited, *Geophysical Research Letters,* Vol. 25, pp. 341-344, 1998.

[Turnbull and Lowe 1988] Turnbull D.N., and Lowe R.P., New hydroxyl transition probabilities and their importance in airglow studies, *Planetary and Space Science,* Vol. 37, No.6, pp.723-738,1989.

[Wright 2005] Wright E.L. The infrared sky. *New Astronomy Reviews,* Vol. 49, pp.407-412, 2005.

A Plots

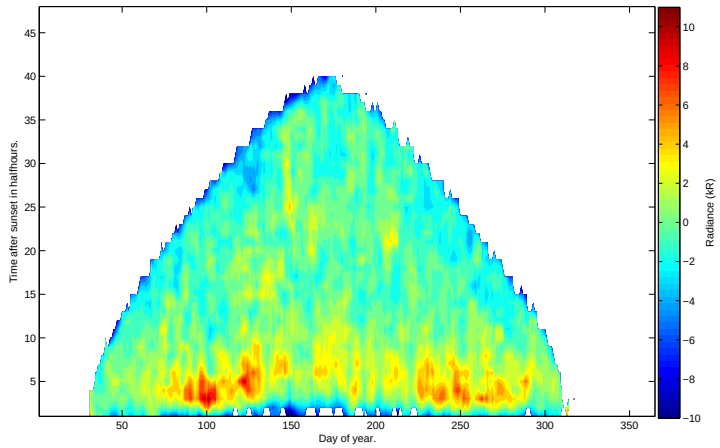

Figure A.1: Development of the average nightly radiance of the OH Meinel (3,1) band after sunset during the year.

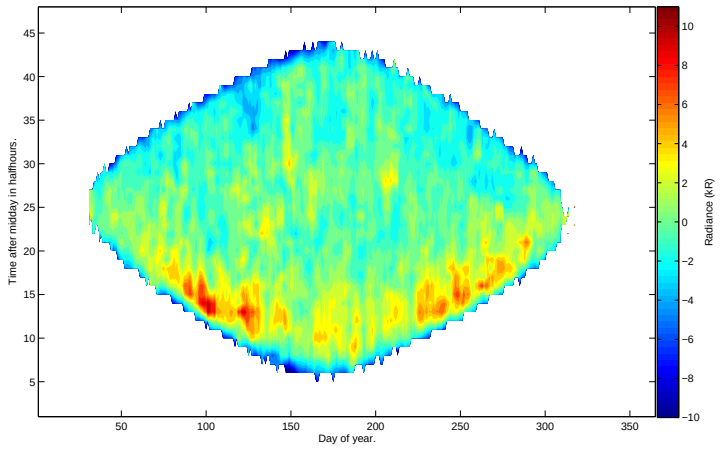

Figure A.2: Development of the average radiance during a night through a year for the OH Meinel (3,1) band.

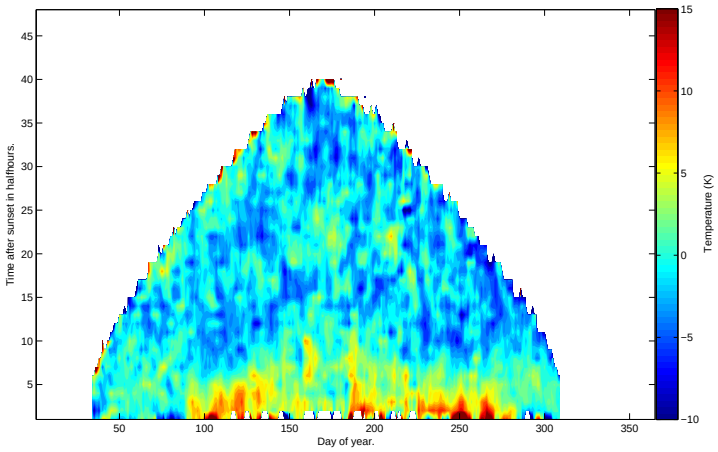

Figure A.3: Development of the average nightly temperature of the OH Meinel (3,1) band after sunset during the year.

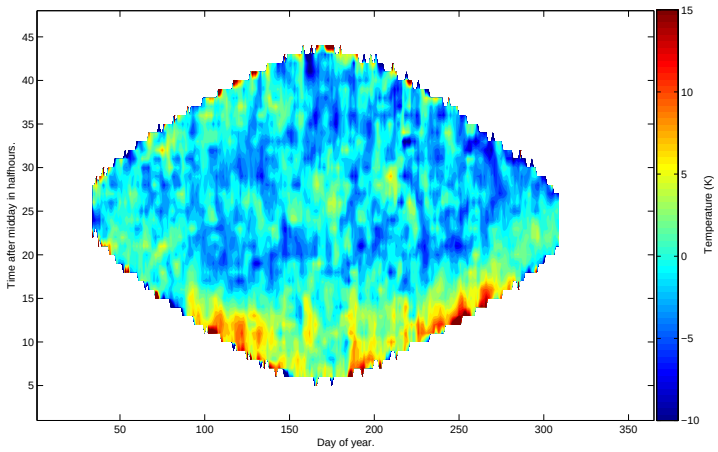

Figure A.4: Development of the average temperature during a night through a year for the OH Meinel (3,1) band.

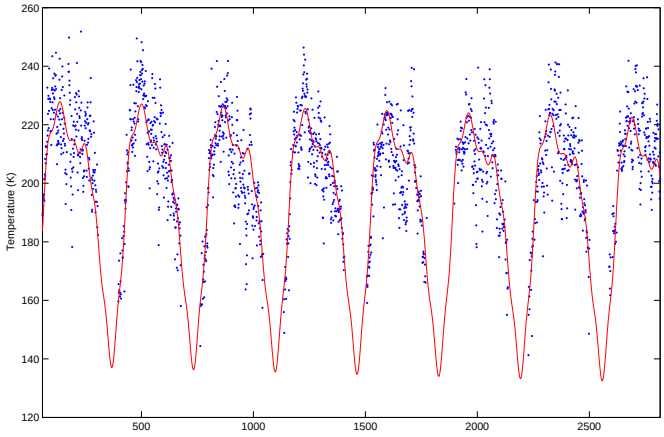

Figure A.5: Temperature of the OH (3,1) band for 2002 to 2009. The fit to the data is shown in red.

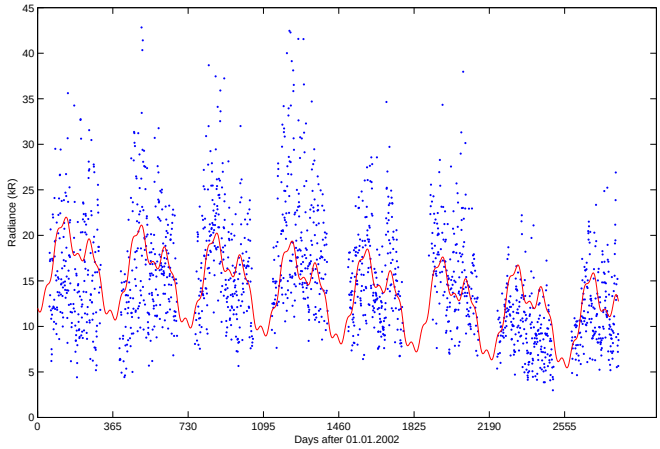

Figure A.6: Radiance of the OH (3,1) band for 2002 to 2009. The fit to the data is shown in red.

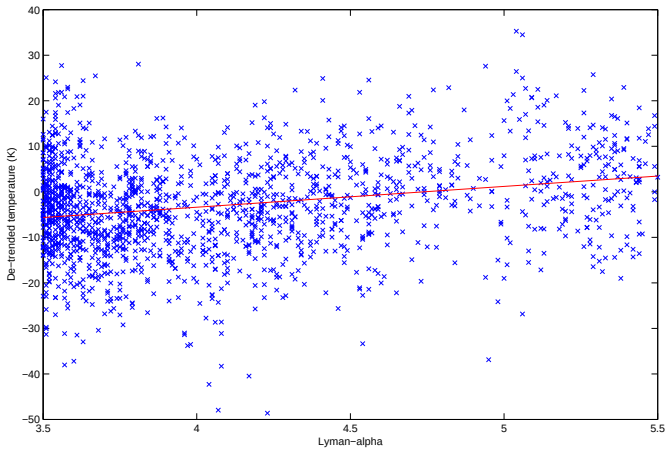

Figure A.7: Correlation between the Lyman-α flux and temperature for the OH Meinel (3,1) band.

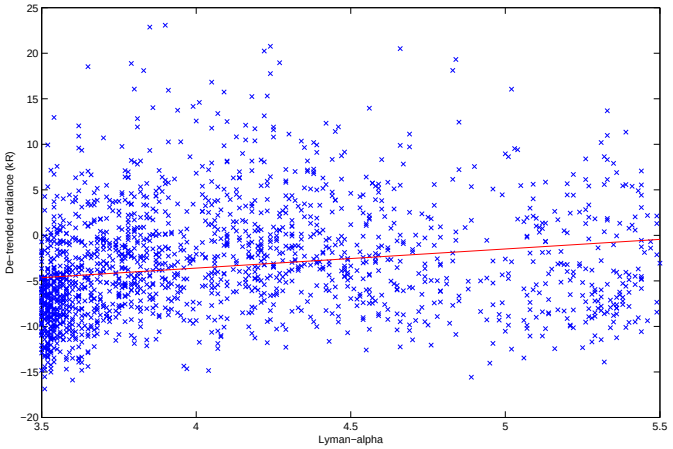

Figure A.8: Correlation between the Lyman-α flux and radiance for the OH Meinel (3,1) band.

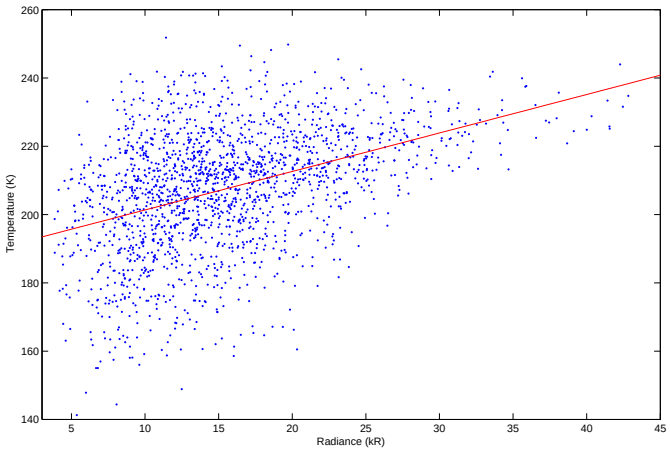

Figure A.9: Temperature of the (3,1) band is plotted against the radiance of the same band.